[22]H. Poincaré, *Science et Methode* (Flammarion, Paris, 1908), p. 96.
[23]S. Themerson, Cardinal Pölätüo (Gaberbocchus, London, 1961), p. 92.
[24]H. B. G. Casimir (private communication, 1986).
[25]D. C. Mattis, *The Theory of Magnetism* (Harper & Row, New York, 1965), p. 38.
[26]J. O. Hirschfelder, C. F. Curtiss, and R. Byron Bird, *Molecular Theory of Gases and Liquids* (Wiley, New York, 1967), p. 960.
[27]B. R. A. Nijboer, Physica A **79**, 420 (1975).
[28]L. Rosenfeld, *Theory of Electrons* (Dover, New York, 1965), p. 14.
[29]P. Mazur and B. R. A. Nijboer, Physica **19**, 971 (1953).
[30]K. Schram, Physica **26**, 1080 (1960).
[31]S. R. de Groot, in *Studies in Statistical Mechanics*, edited by E. W. Montrell and J. L. Lebowitz (North-Holland, Amsterdam, 1969).
[32]F. N. H. Robinson, *Macroscopic Electromagnetism* (Pergamon, Oxford, 1973).
[33]S. R. de Groot and P. Mazur, *Non-Equilibrium Thermodynamics* (North-Holland, Amsterdam, 1962), pp. 22, 83.
[34]S. G. Brush, *Statistical Physics and the Atomic Theory of Matter* (Princeton U.P., Princeton, NJ, 1983).
[35]*Entropy and Information in Science and Philosophy*, edited by L. Kubát and J. Zeman (Elsevier, Amsterdam, 1975).
[36]E. C. G. Stueckelberg de Breidenbach and P. B. Scheurer, Thermocinétique Phénoménologique Galiléenne (Birkhauser, Basel, 1974).
[37]C. Truesdell, *An Idiot's Fugitive Essays on Science* (Springer, New York, 1984).
[38]I. Prigogine, *From Being to Becoming* (Freeman, New York, 1980).
[39]I. Prigogine and I. Stengers, *Order Out of Chaos* (Bantam, New York, 1984).
[40]I. E. Farquhar, *Ergodic Theory in Statistical Mechanics* (Wiley–Interscience, London, 1964).
[41]C. Kittel, *Introduction to Solid State Physics* (Wiley, New York, 1967), 3rd ed., p. 142.

Demonstration of single-electron buildup of an interference pattern

A. Tonomura, J. Endo, T. Matsuda, and T. Kawasaki
Advanced Research Laboratory, Hitachi, Ltd., Kokubunji, Tokyo 185, Japan

H. Ezawa
Department of Physics, Gakushuin University, Mejiro, Tokyo 171, Japan

(Received 17 December 1987; accepted for publication 22 March 1988)

The wave–particle duality of electrons was demonstrated in a kind of two-slit interference experiment using an electron microscope equipped with an electron biprism and a position-sensitive electron-counting system. Such an experiment has been regarded as a pure thought experiment that can never be realized. This article reports an experiment that successfully recorded the actual buildup process of the interference pattern with a series of incoming single electrons in the form of a movie.

I. INTRODUCTION

The two-slit interference experiment with electrons is frequently discussed in textbooks on quantum mechanics, and is referred to as "impossible, absolutely impossible to explain in any classical way, and has in it the heart of quantum mechanics." [1] In this experiment (see Fig. 1), electrons incident on a wall with two slits pass through the slits and are detected one by one on a screen behind them. Accumulation of successive single electrons detected at the screen builds up an interference pattern. According to the interpretation in quantum mechanics, a single electron can pass through both of the slits in a wave form called "probability amplitude" when the uncertainty of the electron position in the wall plane covers the two slits, and when no observation is made of the electron at either one of the slits. The electron is then detected as a particle at a point somewhere on the screen according to the probability distribution of the interference pattern. However, if the electron is caught when passing through the slits, it takes place at either one of the two slits, never both, and the probability distribution on the screen will be completely different.

Although in textbooks this experiment is talked about as a matter of fact, "this experiment has never been done in just this way, since the apparatus would have to be made on an impossibly small scale," as Feynman points out.[1] However, this is not necessarily true. In fact, several attempts have been made up to now; Zeilinger *et al.*[2] confirmed the

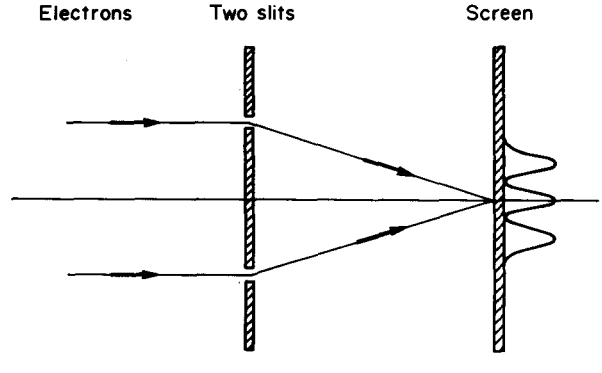

Fig. 1. Two-slit electron interference experiment.

formation of the neutron interference pattern, just as quantum mechanics predicts, by counting arriving neutrons with a scanning counter. In the case of electrons, two groups, one at Tübingen University[3] and the other at Bologna University,[4] demonstrated, in the form of a movie using a highly sensitive TV camera, the observability of the electron interference pattern as it appears when the frequency of incident electrons increases; they showed the electron arrival in each frame without recording the cumulative arrivals. In the case of photons, the buildup process of the interference pattern was recorded on a movie film by Tsuchiya *et al.*[5] with a position-sensitive counter to accumulate the arrival of single photons on the screen. We note that the typical wavelengths of photons are much larger than those of electrons. Therefore, the difficulty Feynman attributes to the two-slit experiments for electrons does not exist for photons.

The present experiment aims at realizing the two-slit thought experiment for electrons in the form of biprism interference.

II. THEORY OF THE BIPRISM INTERFERENCE PATTERN[6]

The principle of the electron biprism invented by Möllenstedt and Dücker[7] in 1956 has been investigated from both geometric- and wave-optical aspects.[7–10] Here, a brief account of the biprism interferometer is given for the reader's convenience.

The biprism consists of two parallel grounded plates with a fine filament between them, the latter having a positive potential relative to the former. If, in the coordinate system shown in Fig. 2, the electrostatic potential is given by $V(x,z)$ and the incoming electron wave by $e^{ik_z z}$, the deflected wave is given by

$$\psi(x,z) = \exp i\left(k_z z - \frac{me}{\hbar^2 k_z}\int_{-\infty}^{z} V(x,z')dz'\right), \qquad (1)$$

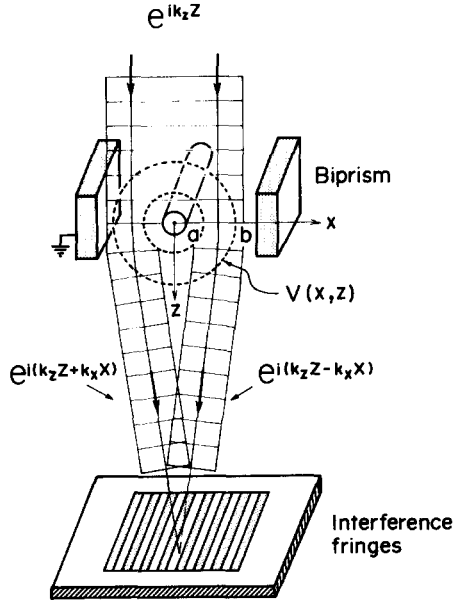

Fig. 2. Deflection of electron waves by biprism—the case of plane-wave incidence.

when $\hbar^2 k_z^2/2m \gg e|V(x,z)|$, as is the case in the present experiment.

The two waves having passed on each side of the filament can be approximated by

$\exp i(k_z z \pm k_x x)$ up to a constant factor, where

$$k_x = -\frac{me}{\hbar^2 k_z}\int_{-\infty}^{\infty}\left(\frac{\partial V(x,z')}{\partial x}\right)_{x=a} dz', \qquad (2)$$

and the symmetry $V(x,z) = V(-x,z)$ has been taken into account. Therefore, the wave fronts of the two waves are deflected as shown in Fig. 2 and, consequently, the waves propagate toward the center, since $k_x > 0$.

This can be interpreted classically also: $-e[\partial V(x,z')/\partial x]_{x=a}$ is the x component of the force exerted on the electron. Its integral with respect to $dz/v_z = dt$, $v_z = \hbar k_z/m$) gives the impulse imparted to it, which is the same in absolute value but reversed in sign, depending on which side of the filament the electron passes.

If the two waves overlap in the observation plane to give

$$\psi(x,z) = e^{ik_z z}(e^{-ik_x x} + e^{ik_x x}), \qquad (3)$$

then this leads to the interference fringes

$$|\psi(x,z)|^2 = 4\cos^2 k_x x. \qquad (4)$$

If the potential in the neighborhood of the filament is approximated by

$$V(x,z) = V_a[\ln(\sqrt{x^2+z^2}/b)/\ln(a/b)], \qquad (5)$$

then

$$k_x = \pi e V_a/\hbar v_z \ln(b/a). \qquad (6)$$

For $v_z = c/2 = 1.5\times10^8$ m/s, $V_a = 10$ V, $a = 0.5$ μm, $b = 5$ mm, $k_x = (\pi/900)$ Å^{-1}, and fringe spacing $d = 900$ Å. In the actual experiment, a spherical wave instead of a plane wave is incident on the biprism and, consequently, the fringe spacing becomes larger, as described in Sec. III.

III. EXPERIMENTS

Experiments were carried out using an electron microscope equipped with an electron biprism and a position-sensitive electron-counting system.

Coherent electron waves from a sharp field-emission tip were, after collimation, sent to an electron biprism. The biprism interference pattern was enlarged by the electron lenses and the single-electron buildup of the interference pattern was observed in time sequence on the TV monitor of a two-dimensional position-sensitive electron-counting system, which was connected to a storage memory. Electrons could be detected one by one, since the detection efficiency was approximately 100% and the detection error was less than 1%.

The detailed experimental arrangement is shown in Fig. 3. Electrons are emitted from a field-emission tip by an applied electrostatic potential $V_1 = 3-5$ kV, and then accelerated to the anode of potential $V_0 = 50$ kV. The electron beam accelerated to V_0 is associated with a wave of wavelength

$$\lambda = h/\sqrt{2meV_0(1+eV_0/2mc^2)}, \qquad (7)$$

which, in the present case, is 0.054 Å. The total emission current is intentionally limited to ~ 1 μA, only 10^{-4} of which passes through the anodes. The electrons are focused through the condenser lens into fine probe P_1, and

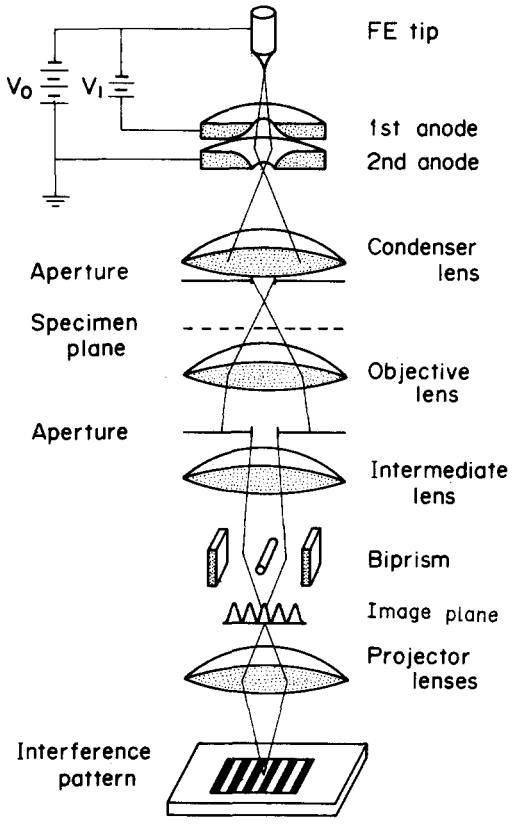

Fig. 3. Electron-optical diagram of the interference experiment.

then illuminate the specimen plane. At this stage, $\frac{1}{10}$ of the electrons pass through the condenser aperture. The electron amplitude in the specimen plane is reproduced through the objective and intermediate lenses onto the image plane of the intermediate lens. Only the central portion of the beam passes through the field-limiting aperture located just above the intermediate lens and is focused by the lens into fine probe P_2. The total current is controlled by changing the focal length of the intermediate lens and, in a typical case, is 1.6×10^{-16} A or 10^3 electrons/s.

The beam issuing from the probe is then incident on the biprism, and the two partial beams are deflected by the angles $\pm k_x/k_z$ [see Eq. (2)] on each side of the biprism. The divergence angle 2α of the incident beam is approximately 4×10^{-8} rad. Consequently, the transverse coherence length given by $\lambda/2\alpha$ is 140 μm, which is larger than the diameter of the biprism filament ($<1\,\mu$m) but smaller than the distance between the two grounded electrodes (~10 mm). The two beams interfere on the image plane to form interference fringes, one-half of the angle β between the interfering beams being given by

$$\beta = l/(l+l')(k_x/k_z)\,, \tag{8}$$

and the fringe spacing by

$$d = \lambda/2\beta\,, \tag{9}$$

which is larger by a factor $(l+l')/l$ than the value given at the end of Sec. II.

In this experiment, $\lambda = 0.054$ Å, $V_a = 10$ V, $l'/l = 6$, and $2\beta = 8\times10^{-6}$ rad, so that $d = 7000$ Å. The interference pattern is finally magnified 2000 times through two projector lenses onto the detector plane. The detector is approximately 12 mm in diameter and the enlarged fringe spacing is 1.4 mm.

Electrons are detected by a two-dimensional position-sensitive electron-counting system, which is schematically illustrated in Fig. 4. This system is a combination of a fluorescent film and the photon-counting image acquisition system (PIAS) produced by Hamamatsu Photonics K.K. We paid special attention to suppressing both counting loss and detection noise to less than 1%. When a 50-kV electron hits the fluorescent film, approximately 500 photons are produced from the spot. The photons excite the photo cathode through the fiber plate and photo electrons are produced. They are accelerated to 3 kV through the electrostatic lens and the point image of electrons is formed at the upper surface of the multichannel plate (MCP). The number of electrons is multiplied there and the position is then measured by the position sensor. The signal of the electron arrival at each channel is transferred to the storage memory and the accumulated electron image is displayed on the TV monitor.

The experiment was performed at the electron arrival rate of approximately 10^3 electrons/s in the whole field of view so that the interference fringes could be formed in a reasonable time, say, 20 min. The distance from the source to the screen is 1.5 m, while the average interval of successive electrons is 150 km. In addition, the length of the electron wave packet is as short as $\sim1\,\mu$m. Therefore, there is very little chance for two electrons to be present simultaneously between the source and the detector, and much less chance for two wave packets to overlap.

An example of the buildup process of the interference pattern is shown in Fig. 5 in the form of a time series of photographs. The photographs were taken from single frames in a TV display. Electrons were detected one by one, and the total number of accumulated electrons increases with time. At first, electrons appear to be distributed quite at random. A dim figure of the biprism fringes begins to emerge in Fig. 5(c). The fringes can finally be clearly observed in Fig. 5(e), where the total number of electrons is approximately 70 000, i.e., 14 000 electrons per fringe.

These results unambiguously demonstrate the wave–particle duality of electrons. On the one hand, a single electron passes through the two slits as a wave and forms a probability interference pattern; electron–electron interaction plays no role in this process since the subsequent elec-

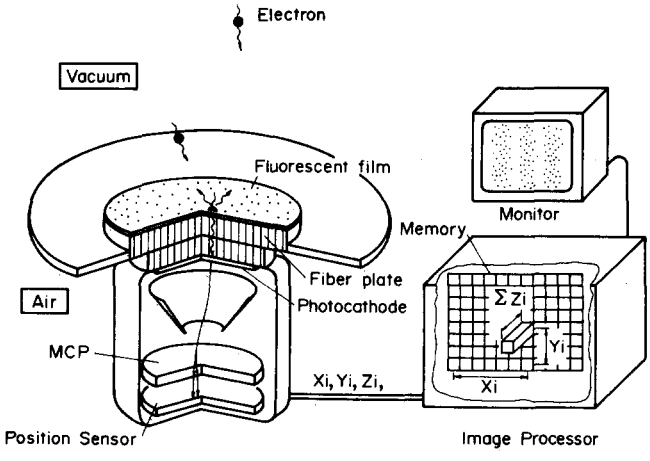

Fig. 4. Schematic diagram of position-sensitive electron-counting system.

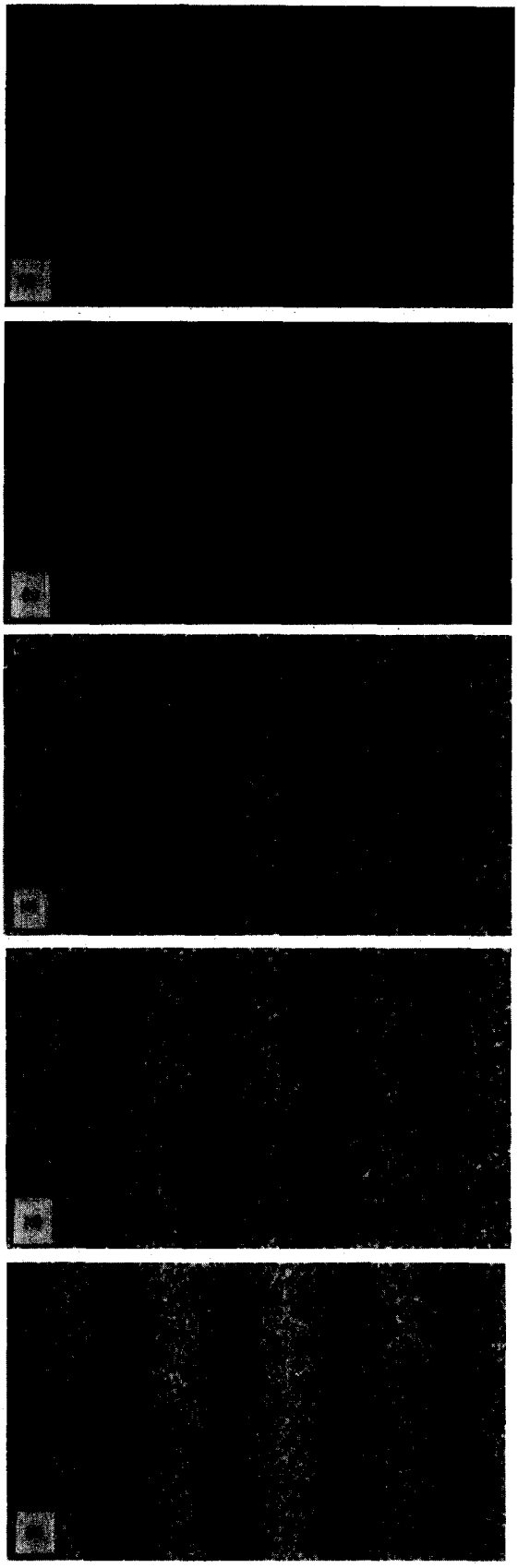

Fig. 5. Buildup of the electron interference pattern. The central field of view, $\frac{1}{3}$ width and $\frac{1}{2}$ length, of the whole field of the detector plane is shown here. The picture extends similarly to the whole field: (a) Number of electrons = 10; (b) Number of electrons = 100; (c) Number of electrons = 3000; (d) Number of electrons = 20 000; and (e) Number of electrons = 70 000.

tron is not even produced from the cathode till long after the preceding electron is detected. At the detector, on the other hand, an electron is observed as a localized particle. We must conclude that a certain position on the screen is selected, onto which the electron wavefunction collapses. The position cannot be predicted, but occurs in the probabilistic way dictated by the probability amplitude.

A series of similar experiments was carried out for different electron intensities ranging from 5000 to 200 electrons/s. The contrast of the fringes obtained remains the same within experimental error of 10%. At the smaller intensity, the error often became large due to the long exposure time, since the error originates mainly from the drift of the biprism filament.

IV. CONCLUSION

We realized a two-slit interference experiment, once regarded as a pure thought experiment with no hope of precise execution, with a combination of both electron-counting and magnifying techniques. The resultant buildup of the interference pattern is exactly as predicted by quantum mechanics.

ACKNOWLEDGMENTS

We should like to thank Dr. Yoshiji Suzuki, Dr. Yutaka Tsuchiya, and Nobuyuki Hirai of Hamamatsu Photonics K.K. for their cooperation in developing the electron detector. Thanks are also due to Dr. Hideo Todokoro of Central Research Laboratory and Shuji Hasegawa of Advanced Research Laboratory, Hitachi, Ltd., for their helpful discussions and assistance in the experiment.

[1] R. P. Feynman, R. B. Leighton, and M. Sands, *The Feynman Lectures on Physics* (Addison-Wesley, Menlo Park, CA, 1965), Vol. III, pp. 1-1–1-5.

[2] A. Zeilinger, R. Gaehler, C. G. Shull, and W. Treimer, in *Proceedings of the Conference on Neutron Scattering, Argonne, 1981*, edited by J. Faber, Jr. (AIP, New York, 1982), p. 93.

[3] The movie was shown in the International Symposium on Foundations of Quantum Mechanics held at Tokyo in 1983, by H. Lichte, Institute of Applied Physics, University of Tübingen, 74 Tübingen, West Germany; see also H. Lichte, in *New Techniques and Ideas in Quantum Measurement Theory*, edited by D. M. Greenberger (New York Academy of Sciences, New York, 1988), p. 175.

[4] The movie was produced by G. Pozzi and G. F. Missiroli, Department of Physics, University of Bologna, 40126 Bologna, Italy.

[5] Y. Tsuchiya, E. Inuzuka, T. Kurono, and M. Hosoda, in *Advances in Electronics and Electron Physics*, edited by P. Hawkes (Academic, New York, 1982), Vol. 64A, p. 21.

[6] H. Ezawa (in preparation).

[7] G. Möllenstedt and H. Dücker, Z. Phys. **145**, 375 (1956).

[8] J. Faget and C. Fert, Cah. Phys. **83**, 285 (1957).

[9] T. Hibi and S. Takahashi, J. Electron Microsc. **12**, 129 (1963).

[10] J. Komrska, V. Drahos, and A. Delong, Opt. Acta **14**, 147 (1967).

The neutron interferometer as a device for illustrating the strange behavior of quantum systems

Daniel M. Greenberger

City College of the City University of New York, New York, New York, 10031

The neutron interferometer is a unique instrument that allows one to construct a neutron wave packet of macroscopic size, divide it into two components separated by centimeters, and then coherently recombine them. A number of experiments clearly showing the difference between quantum and classical theory have been performed with it, which are suitable for presentation in elementary quantum courses. This article presents a simple mathematical model of the interferometer, which can be used to illustrate clearly many of the surprising features of quantum systems. For example, one can describe an experiment to determine which component beam the neutron takes (an analog of the two-slit electron experiment). One can then trace in detail the loss of coherence of the wave function, rather than merely invoke the usual "handwaving" uncertainty arguments. The author discusses the effect of gravity on the neutron beam [the classic COW (Colella, Overhauser, and Werner) experiment], including a simple analysis in an accelerated reference frame, and its relation to the equivalence principle, the red shift, and the twin paradox. Also described are the effect of rotation of the neutron by 360° to change its phase, the effect on the wave function of measuring the absence of the particle from a beam ("Dicke's paradox"), and a realizable version of Wheeler's "delayed-choice" experiments, as well as their relation to the problem of "Schrödinger's cat." The treatment is suitable for bright undergraduates and first-year graduate students.

CONTENTS

I. INTRODUCTION—THE NEUTRON INTERFEROMETER

The neutron interferometer is a truly extraordinary piece of experimental equipment that permits one to perform in the laboratory a number of experiments that check the basic ideas of quantum mechanics. Until the advent of this device many of these experiments would have been described as *Gedankenexperimente,* that is, experiments which point up with particular clarity how the theory indicates particles ought to behave, but which would be so difficult to perform that one must be satisfied with considering them as "thought" experiments.

One of the most important attributes of the neutron interferometer is its conceptual simplicity, which allows one to understand the basic ideas of what is happening without going into a detailed technical description. Of course, as with any real device, there are a number of complicated phenomena taking place inside the interferometer, but to interpret the experiments we shall describe, it is not necessary to consider them. Instead we shall present a simplified model of the interferometer, in terms of which we can follow the neutron beam through it, and from which we can calculate all the results we need. With this model, one can present to students some of the more surprising properties of quantum-mechanical systems, in a way that is relatively easy both to understand and to calculate.

The simplest type of interferometer is constructed from a single crystal[1] [see Fig. 1(a)]. There are three slabs or "ears" cut from the crystal, with enough of the rest of the crystal left to offer structural support. The beam is split into two coherent sub-beams in the first ear, at point A, by Bragg scattering off the atomic planes perpendicular to the face of the crystal [the dotted lines in Fig. (1b)]. In the second ear the beams are redirected, at B and C, and

[1]An introductory overview of the subject, covering the more important experiments, is given in Werner, 1980. Another elementary account appears in Overhauser and Colella, 1980. One with more emphasis on the gravitational experiments is given by Greenberger and Overhauser, 1980. Two review articles that cover the detailed physics inside the interferometer, as well as a wide range of experiments, are Bonse and Graeff, 1977, and Rauch and Petraschek, 1979. A conference report covering the state of the art is Bonse and Rauch, 1979, while a detailed treatment of neutron optics can be found in Klein and Werner, 1983.

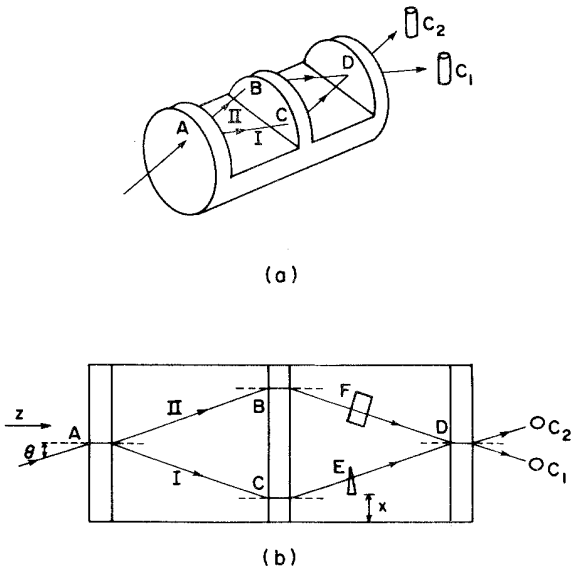

FIG. 1. The neutron interferometer. (a) In the most common type of interferometer three "ears" are cut from the same perfect crystal, ensuring coherence over the entire crystal (about 10 cm long). The incident beam is split at point A into two beams, I and II. These are redirected at B and C and recombined in the last ear at D. The relative phase at D determines the counting rates at the detectors $C1$ and $C2$. (b) The top view of the interferometer. The beam is split by Bragg scattering off the atomic planes perpendicular to the surface of the ear (the dashed lines). The relative phase of the beams I and II can be changed in a known way by inserting a wedge in one beam at E, and varying its thickness by displacing it (varying x). This can be used to determine the phase shift produced by an experiment performed at F.

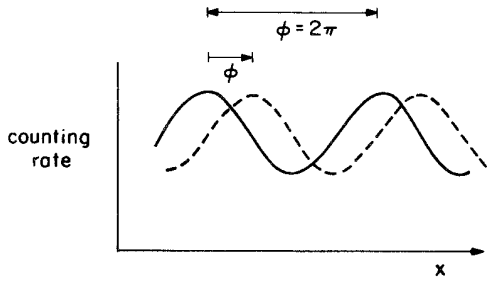

FIG. 2. The interference pattern. By moving the wedge at E in Fig. 1(b), the relative phase between beams I and II is varied. If the counting rate is a maximum in counter $C1$ (and a minimum in $C2$), then altering the relative phase by π will produce a minimum in $C1$ (maximum in $C2$). The counting rate can be plotted against the wedge displacement x, for either counter, yielding an interference pattern. If an experiment is performed at F, the same graph (dashed line) will reveal any extra phase shift ϕ due to the experiment. Since the beams are not totally coherent, the phase cancellation is not perfect, and the minimum intensity will not be zero.

in the third ear they interfere, at D, ultimately going into the two detectors $C1$ and $C2$. The relative counting rates in the detectors determine the relative phasing of the beams. For example, at one particular relative phase, all the neutrons may be entering the counter $C1$. If now the relative phase of the two beams is altered by 180°, corresponding to half a wavelength, then all the neutrons will now enter counter $C2$ (assuming the beams are totally coherent).

An interference pattern can be produced in the following manner. A triangular wedge of matter is placed in the beam I at point E. Because the index of refraction for neutrons will be slightly different from unity inside the matter, the wedge will cause a phase shift. If the counting rate in, for example, counter $C1$ is monitored, it will change as x is varied, because the different wedge thickness will produce a phase shift proportional to Δx. The counting rate can be plotted as a function of x, as in Fig. 2. Then if an experiment is to be performed which alters the phase of beam II at point F by ϕ, the counting rate of $C1$ can again be monitored as a function of x. It is then an easy matter to read off the phase ϕ from the two graphs (including its sign). With some care, the value of ϕ can be determined to within 1°.

The building of such a device became possible with the ability to grow perfect silicon crystals of about 10 cm in length.[2] Thus the atoms in the third ear of the crystal are lined up with those in the first ear, which is what makes coherence over such long distances possible. (Since the crystal spacing is about 1 Å, as is the neutron wavelength, this represents an alignment through about 10^9 λ.) The incident neutron beam need not be terribly well defined, as an extremely accurately defined beam is produced by the interferometer itself for those neutrons which have just the right direction and speed to be Bragg scattered off the planes perpendicular to the crystal face (called Laue scattering). Inside the crystal (see Fig. 3) the forward-scattered beam and backward-scattered beam form a standing wave, which propagates perpendicularly to the crystal face, and at the far end of the crystal, they separate and the forward beam becomes beam II, while the backward-scattered beam becomes beam I. For our purposes we do not need to know any of the details of this process.[3] (Originally, for x rays it was thought the beam would be rapidly absorbed, even at the Bragg angle. This anomalously large transmission process through the crystal is called the Borrmann effect.)

The Laue scattering off the first ear defines the beams I and II within an angular spread $\delta\theta \sim 10^{-6}$ rad (the "Bragg window"). Typical values of the interatomic spacing a are about $a \sim 1$ Å, with λ being given by the Bragg formula $\lambda = 2a \sin\theta$, where the Bragg angle θ is

[2]The first such interferometer was successfully operated for x rays by Bonse and Hart, 1965a, 1965b. It was first applied to neutrons by Rauch, Treimer, and Bonse, 1974.

[3]More of the details of the process are discussed in Greenberger and Overhauser, 1979. A more complete account is given in Squires, 1978, Chap. 6. Two very detailed accounts (for x rays) are James, 1963, and Batterman and Cole, 1964, where the Borrmann effect is especially emphasized.

PHYSICAL REVIEW

LETTERS

VOLUME 66 | 27 MAY 1991 | NUMBER 21

Young's Double-Slit Experiment with Atoms: A Simple Atom Interferometer

O. Carnal and J. Mlynek

Fakultät für Physik, Universität Konstanz, D-7750 Konstanz, Germany

(Received 4 March 1991)

An atomic interferometer based on a Young's-type double-slit arrangement has been demonstrated. A supersonic beam of metastable helium atoms passes through a 2-μm-wide slit in a thin gold foil. This transversely coherent beam impinges on a second microfabricated transmission structure, consisting of two 1-μm-wide slits at a lateral distance of 8 μm. This double slit defines two possible paths on which the atoms can reach the detector slit. The good visibility of the observed fringes should make it possible to measure differential phase shifts in the interferometer of $\frac{1}{3}$ rad in less than 10 min.

PACS numbers: 07.60.Ly, 35.10.−d, 35.80.+s

Matter-wave interferometry is a well established field in physics. Interferometers with de Broglie waves have been demonstrated for electrons and neutrons and extensively used for fundamental tests of quantum-mechanical predictions.[1] The construction of an interferometer for *atoms* is rendered difficult by the fact that atoms carry no charge like electrons and cannot penetrate through condensed matter like neutrons. Therefore novel techniques are required to provide coherent beam splitters for atomic waves. In the last few years, different proposals were published on how to realize an atomic interferometer.[2] In this Letter, we present probably the simplest configuration in which the atoms cover two spatially well separated paths: the quantum-mechanical analog to Young's double-slit interferometer in classical optics (see Fig. 1), which has already been demonstrated for electrons[3] and neutrons.[4] In our arrangement, the slits are mechanical transmission structures with widths in the micrometer range. As atomic species we used metastable helium atoms: The helium atom has a low mass which leads to a large de Broglie wavelength. Moreover, helium is inert, thus facilitating the use of very delicate transmission structures,[5] and the production of an intense helium beam is a well-known technique. In addition, metastable helium atoms are easily detected and have optical transitions in the near infrared, so that their internal and external degrees of freedom can be manipulated by laser fields.

The scheme of our experimental setup is shown in Fig. 2; details of the apparatus are given elsewhere.[5] An intense atomic beam of helium atoms is produced by a supersonic gas expansion. A collinear electron-impact excitation creates metastable atoms in the states 2^1S_0 and 2^3S_1, with relative populations of 90% and 10%, respectively.[6] After the excitation, the beam of metastable atoms has a spectral brightness of $B \cong 10^{17}$ (metastable atoms)/(sec sr cm^2) (Ref. 7) and a velocity ratio of $v_0/\Delta v \cong 15$–20, where v_0 denotes the mean velocity in the beam and Δv the full width at half maximum of the Gaussian velocity distribution. The mean velocity of the atoms, and therefore the mean de Broglie wavelength,

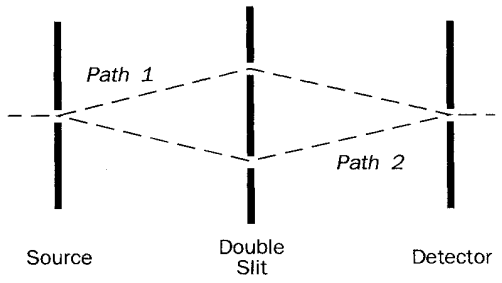

FIG. 1. Scheme of a double-slit interferometer. The atoms can move along two spatially separated paths from the source to the detector.

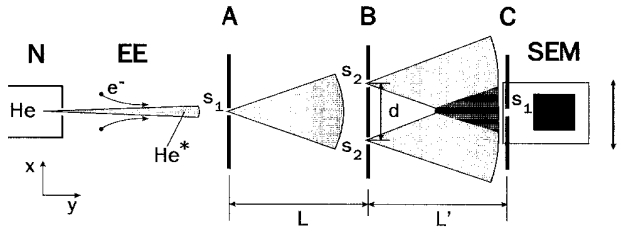

FIG. 2. Schematic representation of the experimental setup: nozzle system and gas reservoir N; electron impact excitation EE; entrance slit A, double slit B, and detector screen C; secondary electron multiplier SEM (mounted together with C on a translation stage). Dimensions: $d=8$ μm, $L=L'=64$ cm; slit widths: $s_1=2$ μm, $s_2=1$ μm.

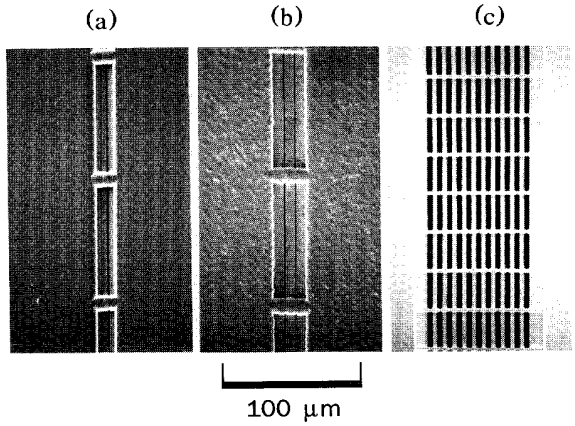

FIG. 3. Scanning-electron-microscope pictures of the microfabricated transmission structures, with the slit structures in the vertical direction and the support gratings in the horizontal direction: (a) entrance and detection slit (slit width $s_1=2$ μm); (b) double slit (slit width $s_2=1$ μm and slit separation $d=8$ μm); (c) detection grating (grating periodicity 8 μm). The 100-μm scale is the same for all three pictures.

can be adjusted by changing the temperature of the gas reservoir and the nozzle system. At present, the reservoir temperature can be set to $T=295$ K, corresponding to a mean de Broglie wavelength of $\lambda_{dB}=0.56$ Å, or to $T=83$ K, corresponding to $\lambda_{dB}=1.03$ Å.

After the electron-impact excitation, the atoms pass through a slit with a width of $s_1=2$ μm, imprinted in a thin gold foil. A scanning-electron-microscope picture of this transmission structure is shown in Fig. 3(a). The total slit height amounts to 4 mm. After having traveled $L=64$ cm downstream, the atoms pass through two 1-μm-wide slits, separated by 8 μm. This double slit is irradiated coherently, as the atomic waves passing the narrow entrance slit are, in analogy to classical optics, transversely coherent over an angle $\theta=\lambda_{dB}/s_1\equiv 5\times10^{-5}$ rad. This double-slit structure [see Fig. 3(b)] is 2 mm high. The edges forming both the entrance and the double slit are 1 μm thick, whereas the surrounding gold foil is 20 μm thick. An additional support grid, having a periodicity of 100 μm and made of 11-μm-wide by 20-μm-thick gold bars, ensures that the edges of each slit are parallel to better than 10^{-4} rad. This support structure reduces the total transmission of the slits by approximately 10%. The atomic waves emerging from the double slit then recombine coherently and produce an interference picture in the atomic density distribution. This density profile is detected in a plane located another $L'=64$ cm behind the double slit. The interference pattern can be monitored either with a 2 μm slit, identical to the entrance slit, or with a grating with a periodicity of 8 μm formed by ten bars [see Fig. 3(c)]. The complete detector system consists of a secondary electron multiplier (SEM) behind a single gold foil with imprinted microfabricated slit and grating, both (SEM and foil) mounted on the same translation stage. The detector system can be moved in steps of 1.88 μm by means of a stepper motor and a precise lead screw. The electronic pulses generated by the SEM are preamplified, discriminated against background noise, and finally added up by a counter. The resulting background noise level of the detector without atomic beam amounted to only 2–3 counts/min. The great number of atoms remaining in the ground state (approximately 10^6 times more than in the two metastable states) does not have any effect on the experiments, since ground-state atoms are not detected. The three successive microfabricated slit structures forming the interferometer were adjusted parallel to better than 5×10^{-4} rad using the diffraction pattern of a 5-mW HeNe laser: For this purpose, the laser beam passed through 20-μm-wide adjustment slits, which are imprinted in the same three gold foils as the transmission structures.

The microfabricated transmission structures were manufactured by Heidenhain Inc., using the manufacturing process "DIAGRID."[8] In this special process, a flat glass substrate is covered with an electrode layer. A thin film of insulating photoresist, put on top of this electrode layer, is structured by a printing process in absolute contact with the original chrome mask. A thin gold film is then deposited by galvanoplating on the photoresist depth profile. No gold accumulates where photoresist is still present. After peeling the gold layer off the substrate, one obtains a gold foil with transmission structures. These thin gold films are finally mounted on flat stainless-steel holders. The gold structures manufactured with this photolithographic technique have extremely precise and steep edges, as shown in Figs. 3(a)–3(c).

The interference pattern, obtained with our double-slit setup, can be calculated to good approximation in the Fraunhofer limit. In the detection plane, we expect a modulated intensity distribution with a periodicity $dx=L'\lambda_{dB}/d$ and an envelope with a full width of $2L'\lambda_{dB}/s_2$;

here d and s_2 are the distance between the two slits and the width of the double slits, respectively. The total number of interference maxima is further reduced by the finite velocity ratio. In a first experiment, we investigated the interference pattern with the single 2-μm slit by moving it laterally to the beam axis in 1.88-μm steps. The integration time at each detector position was 10 min, in order to obtain a reasonable signal-to-noise ratio. The experimental results for two different atomic wavelengths are shown in Figs. 4(a) and 4(b). With a de Broglie wavelength of $\lambda_{dB}=0.56$ Å, the average distance between two maxima is $dx=4.5\pm0.6$ μm [Fig. 4(a)], which agrees well with the theoretical value $dx=L'\lambda_{dB}/d=4.5$ μm. The different interference maxima are not resolved completely, since the interference period is only twice the detector slit width. The scan covers half of the interference pattern, fading out on the right side, due to the finite width of the two slits and the residual velocity spread in the beam. In order to improve the visibility of the fringes we repeated the same experiment, but with a nozzle temperature of $T=83$ K ($\lambda_{dB}=1.03$ Å). In this case, the distance between two maxima increased and was measured to be 8.4 ± 0.8 μm which is close to the theoretical value of 8.2 μm. In Fig. 4(b) we find a visibility V (Ref. 9) of the fringes greater than 60%, if we subtract the detector background. The difference from the expected value of $V=80\%$ could be due to a small misalignment of the three transmission structures or to small-angle collisions of the atoms with the background gas in the vacuum chamber (background pressure $p\cong5\times10^{-7}$ mbar). Since these incoherent processes destroy the phase information between the two paths, this would cause a broad unstructured background signal. Because of the long integration times and a slow thermal drift inside the beam machine, it was not possible with the actual beam intensity to monitor the whole interference pattern in one scan. Nevertheless, the scans displayed in Fig. 4 cover a sufficiently large part of the atomic density distribution, so that the presence of an interference pattern is clearly demonstrated.

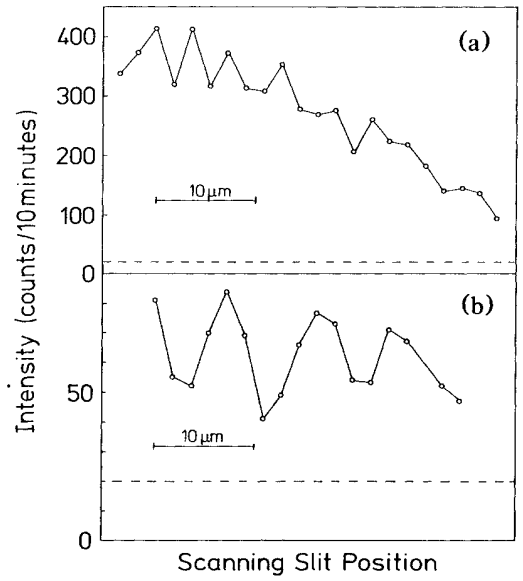

FIG. 4. Measured atomic intensity profiles in the detector plane as a function of the lateral detector position x. The profile is probed with the 2-μm-wide single slit. Atomic wavelength (a) $\lambda_{dB}=0.56$ Å and (b) $\lambda_{dB}=1.03$ Å. The number of detected atoms during 10 min is plotted on the vertical axis. The dashed line is the detector background, with the atomic beam blocked in front of the entrance slit. The line connecting the experimental data is a guide to the eye.

Instead of using a single slit, a grating can be inserted to monitor the intensity distribution. If the grating period and the period of atomic interference pattern coincide, the signal at the detector is maximum when the slits are at positions of the intensity maxima, and a minimum signal occurs when the grating is displaced by half a grating period. Scanning the interference structure with the grating yields an interference picture similar to the one obtained with a single slit in the detector plane [Fig. 4(b)], but with a much higher count rate. For our experimental geometry, the grating period of 8 μm was chosen so that it matched the period of the interference pattern at $L'=64$ cm for $\lambda_{dB}=1.03$ Å. The slits are approximately 4 μm wide, resulting in a grating transmission of 50%. Monitoring the interference pattern with the grating is of interest for applications of this interferometer where only the relative phase between the two different paths and not the actual shape of the interference pattern is important. Figure 5 shows a typical result of an experimental run with the 8-μm grating in the detector plane and a wavelength of $\lambda_{dB}=1.03$ Å. The average distance between two maxima is determined to be 7.7 ± 0.5 μm, which differs from the theoretical value by about 5% and is within the limited accuracy of

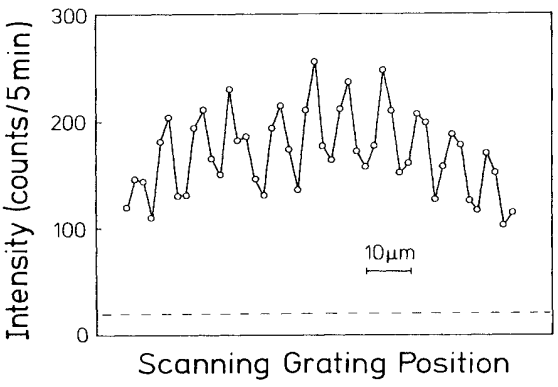

FIG. 5. Atomic density profile, monitored with the 8-μm grating in the detector plane, as a function of the lateral grating displacement. The dashed line is the detector background. The line connecting the experimental points is a guide to the eye.

out setup. The visibility amounts to 30%, whereas 50% can be expected under ideal conditions. The total number of detected atoms is increased by a factor of 10 compared to the case where the interference pattern is monitored with the single slit. With this increase in signal, the integration time could be lowered to 5 min/point, thus reducing the effect of thermal drifts. Since the number n of detected atoms in a given time interval is distributed around a mean number $\bar{n}$ according to Poissonian statistics, the mean relative error at each detector position is given by $1/\bar{n}^{1/2}$. In our case the mean relative error is less than 10% at any detector position; measurements of phase shifts on the order of $\frac{1}{3}$ rad are therefore possible within 10 min.

To improve the signal-to-noise ratio for future experiments, the brightness of the beam has to be increased. Recent experiments have shown that transverse laser cooling of a metastable helium beam can increase the beam intensity by more than a factor of 10.[10] Since a double-slit interferometer is sensitive to a velocity spread in the atomic beam, a very narrow velocity distribution is a prerequisite for precision measurements. Additionally, a larger separation of the double slit is only efficient in connection with an increased velocity ratio. In this respect, investigations by our group on a beam of metastable argon atoms have demonstrated that longitudinal laser cooling in the center-of-mass frame of the atoms can increase the speed ratio in the beam to $v_0/\Delta v > 500$.[11] Thus with present laser cooling techniques, it should be possible to increase the spectral brightness of the He* beam by at least 2 orders of magnitude.

An interferometer of the double-slit type has several applications. Since both paths are spatially separated, it is possible to introduce a relative phase shift between the two arms of the interferometer by applying an external potential to the atoms that varies over the distance between the two paths. Many experiments already carried out with neutrons can be translated to atoms, like tests of the Aharonov-Casher effect, demonstrations of Berry's phase, or measurements of phase changes caused by a rotating or accelerated reference frame.[1] In all these cases, atom interferometry benefits from the larger mass and magnetic moment of atoms compared to neutrons.

Moreover, atom interferometers offer the possibility to investigate various effects due to resonant light-atom interactions. The influence of spontaneous decays on the phase information can be tested, e.g., by irradiating one or both paths with resonant laser light.[12] Another interesting situation arises if an off-resonant laser beam of high intensity induces a pseudopotential for the motion of the atomic center of mass; under appropriate experimental conditions, spontaneous decay processes can then be neglected.

In conclusion, the atomic interferometer presented in this paper is of great simplicity, since all splitting and recombining elements are mechanical structures. Moreover, helium atoms combine many properties that are of great importance when building an interferometer, for example, their low mass and high detection efficiency in the metastable state. First experiments to study laser-induced phase shifts are now in preparation in our laboratory.

We are indebted to T. Sleator for stimulating discussions and for his help during the experiments. We thank H. Kraus in the chemical development department of Heidenhain Inc. for the fabrication of the microstructures and J. Hentschel for the electron-microscope pictures. M. Ammann made decisive contributions to the construction of the beam machine. We also acknowledge many fruitful discussions with A. Faulstich, D. Leipold, and A. Schnetz. This work was supported by the Deutsche Forschungsgemeinschaft.

[1]See, e.g., *Proceedings of the International Workshop on Matter Wave Interferometry, Vienna, 1987,* edited by G. Badurek, H. Rauch, and A. Zeilinger [Physica (Amsterdam) **151B** (1988)].

[2]See, e.g., V. P. Chebotayev, B. Ya. Dubetsky, A. P. Kasantsev, and V. P. Yakovlev, J. Opt. Soc. Am. B **2**, 1791 (1985); P. J. Martin, B. G. Oldaker, A. H. Miklich, and D. E. Pritchard, Phys. Rev. Lett. **60**, 515 (1988); D. W. Keith, M. L. Schattenburg, H. I. Smith, and D. E. Pritchard, Phys. Rev. Lett. **61**, 1580 (1988); J. F. Clauser, Physica (Amsterdam) **151B**, 262 (1988); J. Schwinger, M. O. Scully, and B.-G. Englert, Z. Phys. D **10**, 135 (1988); Ch. J. Bordé, Phys. Lett. A **140**, 10 (1989).

[3]C. Jönsson, Z. Phys. **161**, 454 (1961).

[4]A. Zeilinger, R. Gähler, C. G. Shull, W. Treimer, and W. Mampe, Rev. Mod. Phys. **60**, 1067 (1988).

[5]O. Carnal, A. Faulstich, and J. Mlynek (to be published); A. Faulstich, O. Carnal, and J. Mlynek, in Proceedings of the International Workshop on Light Induced Kinetic Effects on Atoms, Ions and Molecules, Elba, Italy, 1990, edited by L. Moi *et al.* (to be published).

[6]W. Sesselmann, B. Woratschek, J. Küppers, G. Ertl, and H. Haberland, Phys. Rev. B **35**, 1547 (1987).

[7]The spectral brightness B is defined as (particles sr^{-1} time^{-1} area^{-1}) $v/\Delta v$.

[8]The manufacturing process "DIAGRID" is a trademark of Heidenhain Inc. (Traunreut, Germany).

[9]V is defined by $V=(I_{\max}-I_{\min})/(I_{\max}+I_{\min})$, where $I_{\max}$ and $I_{\min}$ denote the maximum and minimum intensities of the interference pattern.

[10]A. Aspect, N. Vansteenkiste, R. Kaiser, H. Haberland, and M. Karrais, Chem. Phys. **145**, 307 (1990).

[11]A. Faulstich *et al.* (to be published).

[12]T. Sleator, O. Carnal, A. Faulstich, and J. Mlynek, Verh. Dtsch. Phys. Ges. (VI) **26**, 867 (1991).

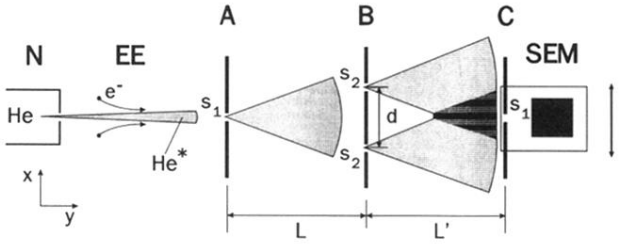

FIG. 2. Schematic representation of the experimental setup: nozzle system and gas reservoir N; electron impact excitation EE; entrance slit A, double slit B, and detector screen C; secondary electron multiplier SEM (mounted together with C on a translation stage). Dimensions: $d = 8\ \mu$m, $L = L' = 64$ cm; slit widths: $s_1 = 2\ \mu$m, $s_2 = 1\ \mu$m.

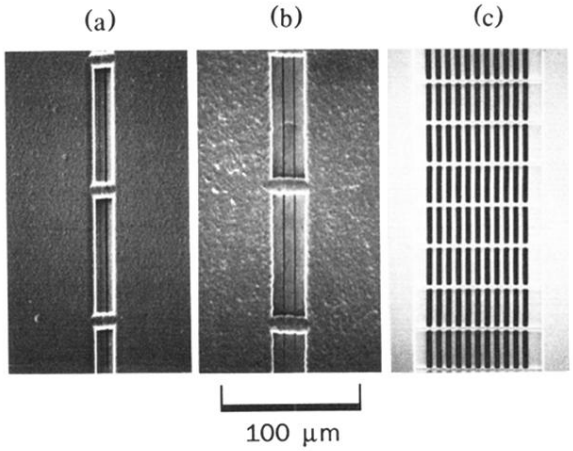

FIG. 3. Scanning-electron-microscope pictures of the microfabricated transmission structures, with the slit structures in the vertical direction and the support gratings in the horizontal direction: (a) entrance and detection slit (slit width $s_1 = 2$ μm); (b) double slit (slit width $s_2 = 1$ μm and slit separation $d = 8$ μm); (c) detection grating (grating periodicity 8 μm). The 100-μm scale is the same for all three pictures.

Quantum interference experiments with large molecules

Olaf Nairz,[a] Markus Arndt, and Anton Zeilinger[b]
Institut für Experimentalphysik, Universität Wien, Boltzmanngasse 5, A-1090 Wien, Austria

(Received 27 June 2002; accepted 30 October 2002)

Wave–particle duality is frequently the first topic students encounter in elementary quantum physics. Although this phenomenon has been demonstrated with photons, electrons, neutrons, and atoms, the dual quantum character of the famous double-slit experiment can be best explained with the largest and most classical objects, which are currently the fullerene molecules. The soccer-ball-shaped carbon cages C_{60} are large, massive, and appealing objects for which it is clear that they must behave like particles under ordinary circumstances. We present the results of a multislit diffraction experiment with such objects to demonstrate their wave nature. The experiment serves as the basis for a discussion of several quantum concepts such as coherence, randomness, complementarity, and wave–particle duality. In particular, the effect of longitudinal (spectral) coherence can be demonstrated by a direct comparison of interferograms obtained with a thermal beam and a velocity selected beam in close analogy to the usual two-slit experiments using light.

[DOI: 10.1119/1.1531580]

I. INTRODUCTION

At the beginning of the 20th century several important discoveries were made leading to a set of mind-boggling questions and experiments that seemed to escape any answers based on classical, pre-quantum physics. The first were the discoveries[1–3] that implied that optical radiation has to be composed of discrete energy packages that can be well localized in space and time. This localization was in marked contrast to the existing knowledge based on Maxwell's theory which successfully represented light as electromagnetic waves. The second and complementary breakthrough was the theoretical result by de Broglie,[4] and the experimental demonstration by Davisson and Germer[5] that massive particles also propagate in a wave-like manner.

Both statements were stunning at the time that they were proposed and both keep us busy thinking even today because we generally associate the notion of point-like locality with a particle while we attribute spatial extension to a wave. The observation of both phenomena in one and the same experiment leads us also to the concept of delocalization, which goes beyond the simple concept of ''being extended,'' because single quantum objects seem to be able to simultaneously explore regions in space–time that cannot be explored by a single object in any classical way.

To illustrate the wave–particle duality we shall briefly recall the double-slit experiment as sketched in Fig. 1 because it is both one of the simplest and most general quantum experiments used in introductory quantum physics and is the prototype for our studies with molecules.

Let us first discuss an experiment that is usually performed in a ripple tank. If we excite surface waves in water and let them propagate through a small hole in a barrier (Fig. 1, left), we would observe a circular wavelet emerge behind the barrier in agreement with Huygens' principle. If we now open a second hole in the barrier, we could create regions where the water remains completely still (Fig. 1, center). This phenomenon is simply explained by the fact that the surface waves superpose on each other and the wave minima can be filled by wave maxima at well-determined places. We call this phenomenon interference. It can only be easily observed if the disturbances in the two slits are synchronized with each other, which means that they have a well-defined and constant phase relation, and may therefore be regarded as being coherent with respect to each other.

For water the picture appears intuitive because the wave is composed of many particles, each interacting with its neighbors. But the experiment turns into the mind-boggler mentioned above if we repeat it with an ensemble of isolated objects—photons or even massive particles—which we send through the double-slit one by one.

We shall present experimental results with, at present, the most massive particles that exhibit wave properties. The results confirm that under appropriate circumstances we still obtain interference patterns, the shape of which can be predicted with certainty. However, it is important to note that in such investigations a single particle always gives a single click at one detector position only, and we have no means of calculating the position of this event in advance because, as far as we can tell, it is governed by chance.

Therefore, the double-slit experiment with single particles leads us to the following questions: How can a single particle, which we observe both in the source and in the detector as being well-localized and much smaller than a single opening in the barrier, acquire information about the state (open/closed) of a very remote opening, if it were considered to pass only one through the openings? Why can't we track the particle position without destroying its wave nature? How can we understand the emergence of a well-defined interference pattern in contrast to the random hitting point of the single object if none of the particles can interact with the rest of the ensemble in any way that we know?[6]

We thus find many fundamental quantum concepts in the context of double-slit interferometry. First, we find the complementarity between our knowledge about the particle's position and the visibility of the interferogram. If we open one slit only, the particle must pass this opening and the interference pattern must disappear. Perfect interference contrast can be obtained only if we open the second slit and if we exclude all possibilities of detecting, even in principle, the path the object has taken. The wave–particle duality states that the description of one and the same physical ob-

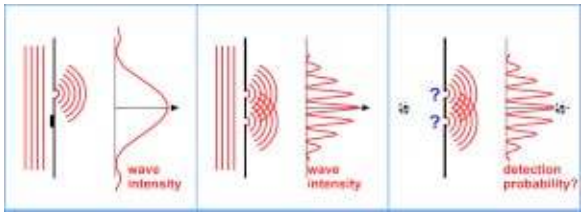

Fig. 1. The double-slit experiment is the prototype experiment demonstrating the wave–particle duality in quantum mechanics. (a) A wave impinging on a wall with one sufficiently small slit will spread out behind this obstacle. An explanation based on Huygen's principle tells us that each point in the wave front can be imagined as being a source of a spherical wavelet. The fields of many such sources interfere on the screen and form the single slit pattern. (b) If we open a second slit, which sees the same wave as the first one, the field amplitude at a sufficiently long distance from the slits drops to zero at specific points: we observe destructive interference due to the overlap of wave troughs and hills. (c) Which pattern can we expect if we replace the continuous source by one that emits quanta, that is, discrete packages of energy and/or mass that are well localized in space and time in the source? Can a single particle as massive as a buckyball acquire information of two spatially separate locations?

ject suggests the local particle picture in the source and on the screen, but a wave model for the unobserved propagation of the object. Mathematically we describe the state of the particle during the propagation as a superposition of states, in particular of position states, that are classically mutually exclusive. A classical object will either take one or the other path. A quantum object cannot be said to do that. The intrinsic information content of the quantum system itself is insufficient to allow such a description—even in principle.[7] We also find the duality between objective randomness and determinism. The pattern on the screen is well determined for the ensemble, but the detection point of a single object is completely unpredictable in all experiments.

All of these ''quantum mysteries'' imply that in an experiment the possibility of having a position is often the only objective reality in contrast to the property of having a well-defined position.

These reasons are why Richard Feynman emphasized that the double-slit experiment is at the heart of quantum mechanics:[8] ''In reality, it contains the only mystery, the basic peculiarities of all of quantum mechanics.'' We might suggest that another central issue of quantum physics, namely entanglement, is missing in this example. However, it turns out to be an essential ingredient if we consider how we could diffuse which-path information to the environment—a phenomenon leading to loss of coherence between the neighboring paths in the double-slit experiment.

The fact that the wave nature of matter is a cornerstone of quantum mechanics, but that this very feature completely escapes perception in our everyday life, is one of the remarkable properties of this theory. The smallness of Planck's constant and therefore of the de Broglie wavelength of a macroscopic object is certainly largely responsible for the nonobservability of quantum effects in the classical world. However, it is interesting to ask whether there are limits to quantum physics and how far we can push the experimental techniques to visualize quantum effects in the mesoscopic world for objects of increasing size, mass, and complexity.

We shall therefore briefly review the experimental efforts in this field throughout the last century. Soon after Louis de Broglie's proposed wave hypothesis for material particles, matter wave phenomena were experimentally verified for electrons,[5] atoms and dimers,[9] and neutrons.[10,11] Young's double-slit experiment with matter waves was then done by Jönsson for electrons,[12] by Zeilinger and collaborators for neutrons,[13] by Carnal and Mlynek for atoms,[14] and by Schöllkopf and Toennies for small molecules and noble gas clusters.[15,16]

Further advances in matter wave physics with atoms were made possible by sophisticated techniques exploiting the interaction between atoms and light. Already in 1975 ideas were put forward for slowing and cooling of atoms using light scattering.[17,18] The rapid progress of this field was recognized by the fact that the most important developments in this field were recently awarded the Nobel prize for laser cooling[19–21] in 1997 and for the experimental realization of Bose–Einstein condensates with dilute atomic vapor[22,23] in 2001. In Bose–Einstein condensates all atoms have extremely long de Broglie wavelengths and are coherent over macroscopic distances up to a millimeter. However, similar to light quanta in a laser beam, the atoms in a Bose–Einstein condensate are kept sufficiently apart to keep their interaction weak. Therefore, in spite of the large coherence length, the interfering object is still of small mass and complexity. Even experiments demonstrating interference between two Bose–Einstein condensates[24] can be viewed as a double-slit experiment with many individual atoms, as witnessed also by the fact that to explain the fringe spacing the de Broglie wavelength corresponding to the individual atom rather than a wavelength using the total mass of the condensate is used.

Different questions and new experimental challenges arise if we study particles in the almost opposite parameter regime where the interaction among the particles is much stronger. Covalently bound atoms form a new entity, a molecule or cluster, and the de Broglie wavelength of this system is defined by the total mass of all the atoms and by the center-of-mass velocity of the bound system. In the following we shall focus on these complex objects.

The very first demonstration of molecule interference dates back to the days of Estermann and Stern[9] in 1930, who demonstrated experimentally diffraction of H_2 at a LiF crystal surface. Further experiments with diatomic molecules had to await progress and interest in atom optics. A Ramsey-Bordé interferometer was already realized for the iodine dimer in 1994[25] and was recently used[26] for K_2. Similarly, a Mach–Zehnder interferometer was demonstrated[27] for Na_2. The near-field analog to the Mach–Zehnder interferometer, a Talbot–Lau interferometer, was recently applied to experiments with Li_2.[28] Diffraction at nanofabricated gratings also turned out to be the most effective way to prove the existence of the weakly bound helium dimer[16] and to measure its binding energy.[29]

Based on these historical achievements we ask how far we might be able to extend such quantum experiments and for what kind of objects we might still be able to show the wave–particle duality. Recently, a new set of experiments exceeding the mass and complexity of the previously used objects by about an order of magnitude has been developed in our laboratory. These experiments with the fullerene molecule C_{60} will be described in Sec. II.

II. THE C_{60} EXPERIMENT

The cage-like carbon molecules earned their names ''fullerenes'' and ''buckminster fullerenes'' because of their close resemblance to geodesic structures that were first discussed by Leonardo da Vinci[30] and implemented in buildings

Fig. 2. The fullerene molecule C_{60}, consisting of 60 carbon atoms arranged in a truncated icosahedral shape, is the smallest known natural soccer ball.

in the United States by the architect Buckminster Fuller.[31] This new modification of pure carbon was discovered in 1985 by Kroto *et al.*[32] and shown to be particularly stable and abundant when exactly 60 carbon atoms are arranged in one molecule to form the smallest natural soccer ball we know, the buckyball, as shown in Fig. 2.

Fullerenes are appealing candidates because a successful quantum experiment with them would be regarded as an important step toward the realm of our macroscopic world: Many of the known physical properties of buckyballs are more closely related to a chunk of hot solid material than to the cold atoms that have so far been used in matter wave interference. The existence of collective many-particle states like plasmons and excitons, the rich variety of vibrational and rotational modes as well as the concept of an internal molecular temperature are only some of the clear indicators of the multiparticle composition of the fullerenes. And we might wonder whether this internal complexity could spoil the quantum wave behavior of the center of mass motion.

To answer this question, we have set up a new experiment as shown in Fig. 3. It resembles very much the standard Young's double-slit experiment. Like its historical counterpart, our setup also consists of four main parts: the source, the collimation, the diffraction grating, and the detector.

A. The source

To bring the buckyballs into the gas phase, fullerene powder is sublimated in a ceramic oven at a temperature of about 900 K. The vapor pressure is then sufficient to eject molecules, in a statistical sequence, one by one through a small slit in the oven. The molecules have a most probable velocity v_{mp} of about 200 m/s and a nearly thermal velocity spread of $\Delta v/v_{\mathrm{mp}} \simeq 60\%$. Here Δv is the full width of the distribution at half height.

To calculate the expected diffraction angles, we first need to know the de Broglie wavelength which is uniquely determined by the momentum of the molecule

$$\lambda = \frac{h}{mv}, \tag{1}$$

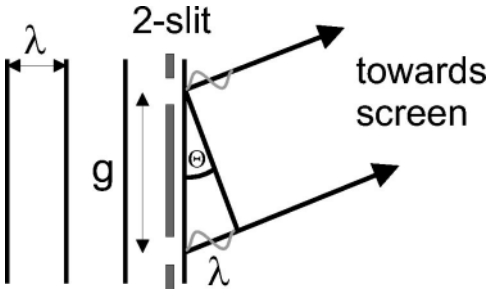

Fig. 4. Textbook approach to double-slit diffraction. First-order interference maxima of a monochromatic wave are caused by constructive interference of the wavelets that emerge from two neighboring slits. The corresponding path length difference between the two paths is equal to the de Broglie wavelength. Higher order interference will be spoiled by the limited longitudinal coherence in a thermal source. Velocity selection in our experiments increases the longitudinal coherence length by more than a factor of 3 and therefore permits the observation of higher order interference fringes.

where h is Planck's constant. Accordingly, for a C_{60} fullerene with a mass of $m = 1.2 \times 10^{-24}$ kg and a velocity of $v = 200$ m/s, we find a wavelength of $\lambda = 2.8$ pm.[33]

B. The diffractive element

Because the de Broglie wavelength is about five orders of magnitude smaller than any realistic free-standing mechanical structure, we expect the characteristic size of the interference phenomena to be small. A sophisticated machinery is therefore necessary to actually show them. As the diffracting element we used a free-standing silicon nitride grating with a nominal grating constant of $d = 100$ nm, slit openings of $s = 55 \pm 5$ nm and thickness of only 200 nm along the beam trajectory. These gratings are at the cutting edge of current technology and only a few specialists worldwide can actually make them.[34]

We can now calculate the deflection angle to the first diffraction order in the small angle approximation as the ratio of the wavelength and the grating constant,

$$\theta = \frac{\lambda}{d} = \frac{2.8 \times 10^{-12}\,\mathrm{m}}{10^{-7}\,\mathrm{m}} = 28\ \ \mu\mathrm{rad}. \tag{2}$$

In elementary textbooks Eq. (2) is usually derived using Fig. 4 and noting that the first constructive interference occurs when the difference between two neighboring paths is equal to one de Broglie wavelength. Because our detector is placed at 1.2 m downstream from the grating, the separation between the interference peaks at the detector amounts then to only $L \times \theta = 1.2\ \mathrm{m} \times 28\ \mu\mathrm{rad} = 34\ \mu\mathrm{m}$.

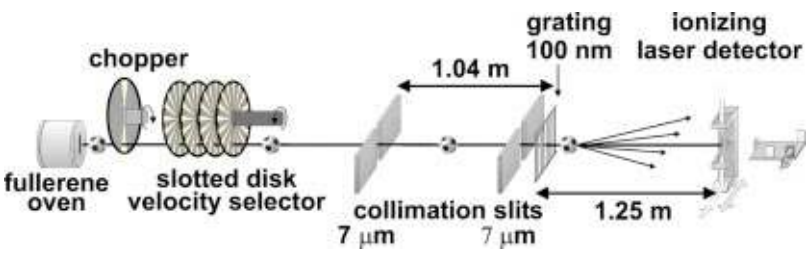

Fig. 3. Setup of the diffraction experiment. Fullerene molecules are sublimated in the oven at 900 K. The spectral coherence can be improved using a mechanical velocity selector. Two collimating slits improve the spatial coherence and limit the angular spread of the beam to smaller than the expected diffraction angle. A SiN grating with a 100 nm period and 50 nm openings is used to diffract the incident molecular waves. The molecular far-field distribution is observed using a scanning laser-ionization detector.

C. The detector

The small spacing between the interference orders requires a high spatial resolution of the molecule detector. For the fullerenes we have implemented a novel detector that surpasses most other schemes in detection efficiency, spatial resolution, and simplicity.

A continuous-wave green laser beam (argon ion laser, all lines) with a full power of 25 W is focused to the beam width of only 4 μm. As shown in Fig. 3, the laser beam is orthogonal to the molecular beam. All molecules that pass the laser beam at or very close to the focus are heated to an internal temperature in excess of 3000 K and ionize. The positive fullerene ions are then accelerated toward an electrode at 10 kV where they induce the emission of electrons. The electrons in turn are again multiplied and the charge pulses are subsequently counted. The overall molecule detection efficiency is about 10% and thus about two orders of magnitude higher than for example, electron beam bombardment ionization as used in many mass spectrometers. We find that among all gases in our vacuum chamber, the laser detector is only sensitive to fullerenes, due to the particular level scheme and high stability against fragmentation. Because of the tight focusing of the laser beam, the effective width of our detector[35] amounts to only $\sim$8 μm, which is sufficient to resolve the individual diffraction orders. To record a diffraction pattern, we scan the laser across the molecular beam in steps of 2 μm. The interferograms shown below represent molecule counts as a function of the transverse laser position.

D. Coherence considerations

Let us now turn to the coherence properties of our molecular beam. In general, coherence means that there is a fixed and well-defined phase relation in space and time between two or more wave fronts.

The spatial (transverse) coherence of our source is almost negligible right after the oven. Inside the source, the coherence width is actually only of the order of the thermal de Broglie wavelength. As is true in general for extended sources with uncorrelated emitters, the visibility is then reduced by the fact that the many partial interferometers—each starting at one point in the source and forming two trajectories through the double-slit toward a point in the detector—acquire different phase differences along their path to a given spot on the screen.

After the oven, we therefore need to enlarge the spatial coherence width by about five orders of magnitude in order to illuminate at least two neighboring slits coherently. Luckily, the spatial coherence is essentially determined by the geometry of the experiment and grows linearly to a good approximation with increasing distance from the source and with decreasing size of the first collimation slit. This general rule for the influence of collimating elements on transverse coherence is commonly known as the van Cittert–Zernike theorem:[36] the spatial coherence function can be derived from diffraction curves which are determined by the apertures along the molecular beam. The limiting element in our case is the first collimation slit.

Obviously the gain in coherence has to be paid for by a dramatic drop in the count rate because the signal decreases quadratically with the distance from the source and linearly with the size of the slit. Although the first collimating slit alone already provides coherence, we still have to introduce a second collimating slit—in our case also 7 μm wide and about 1 m downstream from the first slit. The reason for this is the requirement that the collimated beam width needs to be significantly smaller than the separation between the diffraction orders behind the grating in order to clearly resolve the diffraction peaks.

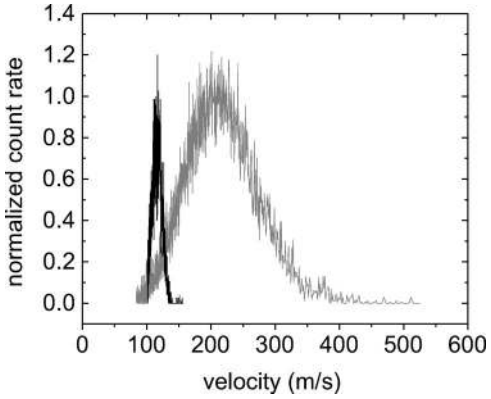

Fig. 5. Velocity distribution of the C_{60} molecules for a thermal and a velocity selected beam. The thermal beam (gray curve) is centered around $\bar{v}=200$ m/s and has a width of $\Delta v/v\sim 0.6$, while the selected beam (black curve) is centered around $\bar{v}=117$ m/s with a width of $\Delta v/v\sim 0.17$. We therefore expect the velocity selected interference pattern to be expanded by 70% on the screen and to show at least three times ($\simeq 0.6/0.17$) as many interference orders as the unselected pattern.

The spectral coherence of the source also enters because molecules with different velocities and therefore different wavelengths follow different diffraction angles. And because the detector records the sum of the correspondingly stretched or compressed diffraction pictures, the interference pattern would be washed out. And in contrast to the spatial contribution, there is no gain in longitudinal (spectral) coherence during free flight. This is due to the fact that different velocity classes will evolve differently. In a pulsed beam experiment we would therefore observe a chirped packet, that is, a wave packet with short wavelengths in the pulse lead and long wavelengths in its tail. And even though the packet would spread out in the course of its evolution, the coherence would not grow due to the internal rearrangement.

Although even in pulsed experiments the spectral coherence does not improve during propagation because of the internal restructuring of the wave packet, the picture of a wave packet is problematic for the description of a continuous source. It is unfounded because the wave packet picture implies a well-defined internal phase structure. More specifically, a wave packet is characterized by a well-defined phase relation between different Fourier components of the beam. Yet such a relation can only be imposed by a suitable preparation. In our case that would imply a well-defined time at which the wave packet starts. This is not provided in our experiment, and the beam can be regarded only as a statistical, and therefore incoherent, mixture of the various momenta. Nevertheless, the beam can operationally be characterized by a coherence length, which is the length that measures the falloff of the interference visibility when the difference between two interfering paths increases. The longitudinal coherence length is given by[37] $L_c\simeq\lambda^2/\Delta\lambda=\lambda v/\Delta v$.

For our thermal beam with $\Delta v/v\sim 0.6$ we find $L_c\sim 1.7\lambda$, which is just enough to guarantee the existence of the first-order interference fringes. We shall later discuss the

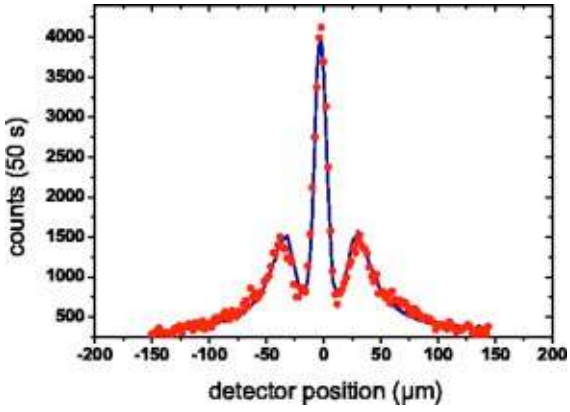

Fig. 6. Far-field diffraction of C_{60} using a thermal beam of $\bar{v}=200$ m/s with a velocity spread of $\Delta v/v \sim 60\%$. The absence of higher order interference fringes is due to the poor spectral coherence.

improvement of the spectral purity using a velocity filter (see Figs. 3 and 5), thereby also improving the wavelength distribution.

Figure 6 shows a typical fullerene diffraction pattern with a thermal beam. We can clearly discern the first interference orders on both sides of the central peak. But the limited coherence is reflected by the fact that we cannot see any second or higher order peaks in the interferogram of Fig. 6.

To see more fringes we have to increase the coherence length and therefore decrease the velocity spread. For this purpose we have employed a mechanical velocity selector, as shown after the oven in Fig. 3. It consists of four slotted disks that rotate around a common axis. The first disk chops the fullerene beam and only those molecules are transmitted that traverse the distance from one disk to the next in the same time that the disks rotate from one open slot to the next. Although two disks would suffice for this purpose, the additional disks decrease the velocity spread even further and help eliminate velocity sidebands. By varying the rotation frequency of the selector, the desired velocity class of the transmitted molecules can be adjusted. To measure the time of flight distribution we chopped the fullerene beam with the chopper right behind the source (see Fig. 3). The selection is of course accompanied by a significant loss in count rate, but we can still retain about 7% of the unselected molecules.

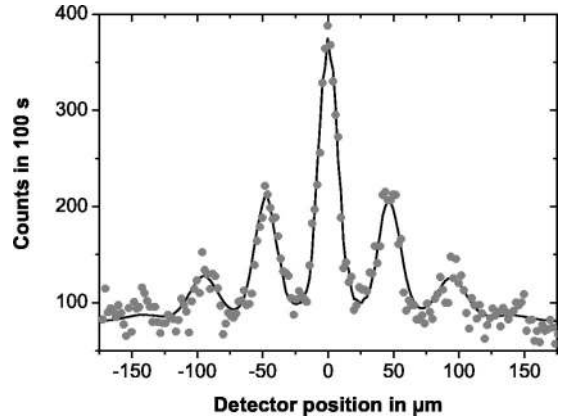

Fig. 7. Far-field diffraction of C_{60} using the slotted disk velocity selector. The mean velocity was $\bar{v}=117$ m/s, and the width was $\Delta v/v \sim 17\%$. Full circles represent the experimental data. The full line is a numerical model based on Kirchhoff–Fresnel diffraction theory. The van der Waals interaction between the molecule and the grating wall is taken into account in form of a reduced slit width. Grating defects (holes) additionally contribute to the zeroth order.

In Fig. 5 both the thermal and the selected velocity distributions are shown. In contrast to the width of the thermal spectrum, amounting to $\Delta v/v=60\%$, we are able to reduce this number to only 17% with the selector. The increase in longitudinal coherence by a factor of more than 3 allows for the observation of diffraction peaks up to at least the second and possibly the third order, as can be seen in Fig. 7.

It should also be pointed out that by using the velocity selector, we can now choose a slow mean velocity centered about 120 m/s, which corresponds to a de Broglie wavelength of 4.6 pm. It is obvious that this increase in wavelength results in a wider separation of the diffraction peaks, which can be seen by comparing Figs. 6 and 7.

In principle, the diffraction patterns can be understood quantitatively within the Fraunhofer approximation of Kirchhoff's diffraction theory as it can be found in any optics textbook.[38] However, Fraunhofer's diffraction theory in the context of optics misses an important point that becomes evident in our experiments with matter waves and material gratings: the attractive interaction between molecule and wall results in an additional phase of the molecular wave function after the passage of the molecule through the slits.[39] Although the details of the calculations are somewhat involved,[40] it suffices here to say that the qualitative effect of this attractive force can be understood as a narrowing of the real slit width toward an *effective* slit width. For our fullerene molecules the reduction can be as big as 20 nm for the unselected molecular beam and almost 30 nm for the velocity selected beam. The stronger effect on slower molecules can be understood by the longer and therefore more influential interaction between the molecules and the wall. However, a complete description would need to take into account the correct shape of the complex (imaginary and real) transmission function, which implies the position-dependent modulation of both the molecular amplitude and phase.

The full lines in Figs. 6 and 7 are fits of our data to this modified Kirchhoff–Fresnel theory. To obtain such a good fit we also have to take into account an enhanced contribution in the zeroth order which we attribute to mechanical defects (holes) of the grating which are significantly larger than the grating period.

III. CONCLUDING REMARKS

A. Single particle interferometry

It is important to note that the interference pattern is built up from single, separate particles. There is no interference *between* two or more particles during their evolution in the apparatus. Single particle interference is evidenced in our case by two independent arguments.

The first argument is based on the spatial separation between the molecules. The molecular flux at an average speed of 200 m/s is $\sim 3\times 10^9$ cm^{-2} s^{-1} at the plane of the detector. This flux corresponds to an average molecular density of 1.7×10^{11} m^{-3} or an average molecular distance of 200 μm. This is three orders of magnitude wider than any realistic range of molecular (van der Waals) forces, which are typically confined to several 100 nm.

The second argument is based on the fact that interference occurs only between indistinguishable states. However, all molecules may be regarded as being in different states. There

are 174 different vibrational modes and the rotational modes can be populated at different energies. The chance of having two subsequent molecules in exactly the same state of all internal modes is vanishingly small. Therefore, interference in our experiments really is a single particle phenomenon!

B. Coherence and which-path information

We might believe that coherence experiments could be spoiled by transitions between the many thermally excited states. Obviously, this is not the case, as has been shown by our experiments. But why is this so? No matter what we do, we can only observe one of these qualities in its ideal form at any given time. If we tried to locate the particle during its passage through one of the two slits, say by blocking one of the openings, the interference pattern would disappear. This rule still holds if we do not block the slit, but manage to obtain which-path information for example via photons scattered or emitted by the molecules. Sufficiently complex molecules, in contrast to the electrons, neutrons, and atoms used so far, may actually emit radiation[41,42] without any external excitation, because they have stored enough thermal energy when leaving the oven. According to Bohr's rule, the interference pattern must then disappear if the molecules emit a photon with a sufficiently short wavelength which enables the experimenter to measure the location of the emitting molecule with sufficient precision. According to Abbé's theory of the microscope, the photon should have a wavelength shorter than twice the distance between the two slits.

What actually saves the experiment is the weakness of the interaction. The wavelength of the most probably emitted photons is about a factor of 100 larger than the separation between two neighboring slits. And the number of light quanta that actually leak into the environment is still sufficiently small—of the order of one, up to potentially a few photons—and cannot disturb the interference measurably. Therefore, even if the fullerene molecule emits a few photons on its path from the source to the detector, these photons cannot yet be used to determine the path taken by the molecule. In other words, the photon state and the molecule state are not (or only very slightly) entangled because the two possible photon emission states from either path largely overlap. In a sense we may say that the fullerene has no ''memory'' along which path the emission occurred.

C. Conclusion

Quantum phenomena become increasingly important and the limit to which we may be able to confirm all quantum principles experimentally is still an open question. The discussion of our fullerene experiments lets us demonstrate the basic wave–particle duality for the most massive, most complex, and most ''classical'' single object so far. Many of the concepts that we teach our students can be illustrated simply. For instance, the notion of coherence length has a rather intuitive meaning when we compare the spectral width of the source and the number of observed interference fringes.

ACKNOWLEDGMENTS

This work has been supported by the European TMR network, Contract No. ERBFM-RXCT960002, by the Austrian Science Foundation (FWF), within Project Nos. SFB F1505 and START Y177 (MA). ON acknowledges a scholarship by the Austrian Academy of Sciences.

[a]Also at: Université de Genève, GAP-Optique, Rue de l'École-de-Médecine 20, CH-1211 Genève 4.
[b]Electronic mail: zeilinger-office@exp.univie.ac.at

[1]M. Planck, ''Zur Theorie des Gesetzes der Energieverteilung im Normalenspektrum,'' Verh. Dtsch. Phys. Ges. **2**, 237 (1900); English translation: ''On the theory of the energy distribution law of the normal spectrum,'' in *The Old Quantum Theory*, edited by D. ter Haar (Pergamon, New York, 1967), p. 82.
[2]P. Lenard, ''Über die lichtelektrische Wirkung,'' Ann. Phys. (Leipzig) **8**, 149–198 (1902).
[3]A. Einstein, ''Über einen die Erzeugung und Verwandlung des Lichtes betreffenden heuristischen Gesichtspunkt,'' Ann. Phys. (Leipzig) **17**, 132–148 (1905); English translation: A. Arons and M. Peppard, ''Concerning an heuristic point of view toward the emission and transformation of light,'' Am. J. Phys. **33**, 367–374 (1965).
[4]L. de Broglie, ''Waves and quanta,'' Nature (London) **112**, 540–540 (1923).
[5]C. Davisson and L. Germer, ''The scattering of electrons by a single crystal of nickel,'' Nature (London) **119**, 558–560 (1927).
[6]A student, having been taught some elementary statistical physics, would be tempted to answer the second one by analogy with the Galton board. Also there, the trajectory of the single particle appears to be undetermined and still the count rate in each channel would be in agreement with the deterministic laws of classical statistics. But we should note, first of all, that the apparent randomness in this example is only due to the ill-defined initial conditions when we release the ball. Second, if we were to perform such a Galton experiment with two different starting positions, the probability distributions of these experiments would simply add up and interference would never be observed.
[7]C. Brukner and A. Zeilinger, ''Young's experiment and the finiteness of information,'' Philos. Trans. R. Soc. London, Ser. A **360**, 1061–1069 (2002).
[8]R. P. Feynman and A. R. Hibbs, *Quantum Mechanics and Path Integrals* (McGraw-Hill, New York, 1965).
[9]I. Estermann and O. Stern, ''Beugung von Molekularstrahlen,'' Z. Phys. **61**, 95–125 (1930).
[10]H. v. Halban Jnr. and P. Preiswerk, ''Preuve Expérimentale de la Diffraction Des Neutrons,'' C. R. Acad. Sci. Paris **203**, 73–75 (1936).
[11]R. Gähler and A. Zeilinger, ''Wave-optical experiments with very cold neutrons,'' Am. J. Phys. **59**, 316–324 (1991).
[12]C. Jönsson, ''Electron diffraction at multiple slits,'' Am. J. Phys. **42**, 4–11 (1974).
[13]A. Zeilinger, R. Gähler, C. G. Shull, W. Treimer, and W. Mampe, ''Single- and double-dlit diffraction of neutrons,'' Rev. Mod. Phys. **60**, 1067–1073 (1988).
[14]O. Carnal and J. Mlynek, ''Young's double-slit experiment with atoms: A simple atom interferometer,'' Phys. Rev. Lett. **66**, 2689–2692 (1991).
[15]W. Schöllkopf and J. P. Toennies, ''Nondestructive mass selection of small van der Waals clusters,'' Science **266**, 1345–1348 (1994).
[16]W. Schöllkopf and J. Toennies, ''The nondestructive detection of the Helium dimer and trimer,'' J. Chem. Phys. **104**, 1155–1158 (1996).
[17]T. W. Hänsch and A. L. Schawlow, ''Cooling of gases by laser radiation,'' Opt. Commun. **13**, 68–69 (1975).
[18]D. Wineland and H. Dehmelt, ''Proposed $10^{14}\Delta\nu<\nu$ laser fluorescence spectroscopy on Tl^+ mono-ion oscillator III (side band cooling),'' Bull. Am. Phys. Soc. **20**, 637–637 (1975).
[19]S. Chu, ''The manipulation of neutral particles,'' Rev. Mod. Phys. **70**, 685–706 (1998).
[20]C. N. Cohen-Tannoudji, ''Manipulating atoms with photons,'' Rev. Mod. Phys. **70**, 707–719 (1998).
[21]W. D. Phillips, ''Laser cooling and trapping of neutral atoms,'' Rev. Mod. Phys. **70**, 721–741 (1998).
[22]M. H. Anderson, J. R. Ensher, M. R. Matthews, C. E. Wieman, and E. A. Cornell, ''Observation of Bose–Einstein condensation in a dilute atomic vapor,'' Science **269**, 198–201 (1995).
[23]K. B. Davis, M.-O. Mewes, M. R. Andrews, N. J. van Druten, D. S. Durfee, D. M. Kurn, and W. Ketterle, ''Bose–Einstein condensation in a gas of Sodium atoms,'' Phys. Rev. Lett. **75**, 3969–3973 (1995).
[24]M. R. Andrews, C. Townsend, H. Miesner, D. Durfee, D. Kurn, and W. Ketterle, ''Observation of interference between two Bose condensates,'' Science **275**, 637–641 (1997).
[25]C. Bordé, N. Courtier, F. D. Burck, A. Goncharov, and M. Gorlicki, ''Molecular interferometry experiments,'' Phys. Lett. A **188**, 187–197 (1994).
[26]C. Lisdat, M. Frank, H. Knockel, M.-L. Almazor, and E. Tiemann, ''Re-

alization of a Ramsey–Bordé matter wave interferometer on the K_2 molecule,'' Eur. Phys. J. D **12**, 235–240 (2000).
[27]M. S. Chapman, C. R. Ekstrom, T. D. Hammond, R. A. Rubenstein, J. Schmiedmayer, S. Wehinger, and D. E. Pritchard, ''Optics and interferometry with Na_2 molecules,'' Phys. Rev. Lett. **74**, 4783–4786 (1995).
[28]See comment by J. Clauser in *Atom Interferometry*, edited by P. R. Berman (Academic, New York, 1997), p. 143.
[29]R. E. Grisenti, W. Schollkopf, J. P. Toennies, G. C. Hegerfeldt, T. Kohler, and M. Stoll, ''Determination of the bond length and binding energy of the Helium dimer by diffraction from a transmission grating,'' Phys. Rev. Lett. **85**, 2284–2287 (2000).
[30]L. Saffaro, ''Cosmoids, fullerenes and continuous polygons,'' in *Proceedings of the First Italian Workshop on Fullerenes: Status and Perspectives*, edited by C. Taliani, G. Ruani, and R. Zamboni (World Scientific, Singapore, 1992), Vol. 2, p. 55.
[31]R. W. Marks, *The Dymaxion World of Buckminster Fuller* (Southern Illinois U.P., Carbondale, 1960).
[32]H. Kroto, J. Heath, S. O'Brian, R. Curl, and R. Smalley, ''C60: Buckminsterfullerene,'' Nature (London) **318**, 162–166 (1985).
[33]It is interesting to compare the de Broglie wavelength of the fullerene with its actual size: The buckyball has a diameter of about 1 nm, which is 350 times larger than its de Broglie wavelength. Our interference experiments clearly show that the concept of the de Broglie wavelength is not merely academic for objects with dimensions much larger than their wavelengths but can actually be demonstrated.
[34]Our gratings were provided by Professor Henry Smith and Dr. Tim Savas of MIT.
[35]M. Arndt, O. Nairz, J. Voss-Andreae, C. Keller, G. van der Zouw, and A. Zeilinger, ''Wave-particle duality of C_{60} molecules,'' Nature (London) **401**, 680–682 (1999); O. Nairz, M. Arndt, and A. Zeilinger, ''Experimental challenges in fullerene interferometry,'' J. Mod. Opt. **47**, 2811–2821 (2000).
[36]For the original work see P. V. Cittert, ''Die wahrscheinliche Schwingungsverteilung in einer von einer Lichtquelle direkt oder mittels einer Linse beleuchteten Ebene,'' Physica (Amsterdam) **1**, 201–210 (1934), and F. Zernike, ''The concept of degree of coherence and its application to optical problems,'' *ibid.* **5**, 785–795 (1938). A textbook with a detailed account of the theorem is M. Born and E. Wolf, *Principles of Optics* (Pergamon, New York, 1993).
[37]L. Bergmann and C. Schaefer, *Optics: Of Waves and Particles* (de Gruyter, New York, 1999).
[38]E. Hecht, *Optics* (Addison-Wesley, Reading, MA, 2002), 4th ed.
[39]This effect has also been described in the context of He diffraction in R. E. Grisenti, W. Schöllkopf, J. P. Toennies, G. C. Hegerfeldt, and T. Köhler, ''Determination of atom-surface van der Waals potentials from transmission-grating diffraction intensities,'' Phys. Rev. Lett. **83**, 1755–1758 (1999).
[40]The van der Waals interaction scales like r^{-3} with the distance r between molecule and grating walls. For C_{60} the scaling even starts to change into a r^{-4} behavior at distances beyond 20 nm, due to the finite (retarded) signaling time between the molecule and its mirror image; see also H. B. G. Casimir and D. Polder, ''The influence of retardation on the London-van der Waals forces,'' Phys. Rev. **73**, 360–372 (1948).
[41]R. Mitzner and E. E. B. Campbell, ''Optical emission studies of laser desorbed C_{60},'' J. Chem. Phys. **103**, 2445–2453 (1995).
[42]K. Hansen and E. Campbell, ''Thermal radiation from small particles,'' Phys. Rev. E **58**, 5477–5482 (1998).

New Journal of Physics
The open-access journal for physics

Toward quantum superposition of living organisms

Oriol Romero-Isart[1,4], Mathieu L Juan[2], Romain Quidant[2,3] and J Ignacio Cirac[1]

[1] Max-Planck-Institut für Quantenoptik, Hans-Kopfermann-Strasse 1, D-85748, Garching, Germany
[2] ICFO-Institut de Ciencies Fotoniques, Mediterranean Technology Park, Castelldefels, Barcelona 08860, Spain
[3] ICREA—Institució Catalana de Recerca i Estudis Avançats, E-08010 Barcelona, Spain
E-mail: oriol.romero-isart@mpq.mpg.de

New Journal of Physics **12** (2010) 033015 (16pp)
Received 4 January 2010
Published 11 March 2010
Online at http://www.njp.org/
doi:10.1088/1367-2630/12/3/033015

Abstract. The most striking feature of quantum mechanics is the existence of superposition states, where an object appears to be in different situations at the same time. The existence of such states has been previously tested with small objects, such as atoms, ions, electrons and photons (Zoller *et al* 2005 *Eur. Phys. J.* D **36** 203–28), and even with molecules (Arndt *et al* 1999 *Nature* **401** 680–2). More recently, it has been shown that it is possible to create superpositions of collections of photons (Deléglise *et al* 2008 *Nature* **455** 510–14), atoms (Hammerer *et al* 2008 arXiv:0807.3358) or Cooper pairs (Friedman *et al* 2000 *Nature* **406** 43–6). Very recent progress in optomechanical systems may soon allow us to create superpositions of even larger objects, such as micro-sized mirrors or cantilevers (Marshall *et al* 2003 *Phys. Rev. Lett.* **91** 130401; Kippenberg and Vahala 2008 *Science* **321** 1172–6; Marquardt and Girvin 2009 *Physics* **2** 40; Favero and Karrai 2009 *Nature Photon.* **3** 201–5), and thus to test quantum mechanical phenomena at larger scales. Here we propose a method to cool down and create quantum superpositions of the motion of sub-wavelength, arbitrarily shaped dielectric objects trapped inside a high-finesse cavity at a very low pressure. Our method is ideally suited for the smallest living organisms, such as viruses, which survive under low-vacuum pressures (Rothschild and Mancinelli 2001 *Nature* **406** 1092–101) and optically behave as dielectric objects (Ashkin and Dziedzic 1987 *Science* **235** 1517–20). This opens up the possibility of testing the quantum nature of living organisms by

[4] Author to whom any correspondence should be addressed.

creating quantum superposition states in very much the same spirit as the original Schrödinger's cat 'gedanken' paradigm (Schrödinger 1935 *Naturwissenschaften* **23** 807–12, 823–8, 844–9). We anticipate that our paper will be a starting point for experimentally addressing fundamental questions, such as the role of life and consciousness in quantum mechanics.

The ultimate goal of quantum optomechanics is to push the motion of macroscopic objects towards the quantum limit, and it is a subject of interest in both fundamental and applied science [4]–[6]. The typical experimental set-up consists of an optical cavity whose resonance frequency depends on the displacement of some mechanical oscillator. The mechanical motion shifts the resonance frequency and, consequently, the radiation pressure exerted into the mechanical object. The overall effect yields the optomechanical coupling, which should enable us to cool down to the ground state the mechanical motion [9]–[11]. We are currently witnessing an experimental race to reach the ground state using different set-ups, such as nano- or microcantilevers [12], membranes [13], or vibrating microtoroids [14]. It is expected that the achievement of the ground state will open up the possibility to perform fundamental and applied experiments involving quantum phenomena with these macroscopic objects, as pioneered by the works [3], [15]–[17].

In this paper, we propose dielectric objects levitating inside the cavity as new quantum optomechanical systems. The fact that these are not attached to other mechanical objects avoids the main source of heating, which is present in other optomechanical systems, and thus, should facilitate the achievement of ground state cooling. Once this is achieved, we propose to create quantum superpositions of the center-of-mass motional state of the object by sending a light pulse to the cavity, which is simultaneously pumped with a strong field. One of the main features of this proposal is that it applies to a wide variety of new objects and, in particular, to certain living organisms. Therefore, our proposal paves the path for the experimental test of the superposition principle with living creatures.

We consider an object with mass M, volume V and relative dielectric constant $\epsilon_r \neq 1$, which may be non-homogeneous. The object is trapped inside a cavity, either by an external trap, provided, for instance, by optical tweezers [18] (figure 1(a)), or by self-trapping using two cavity modes (see appendix D for details). The trap is harmonic, so that the center-of-mass effectively decouples from any relative degree of freedom. Along the cavity axis, this requires the size of the object to be smaller than the optical wavelength that is used for trapping and cooling. The center-of-mass displacement, z, is then quantized as $\hat{z} = z_m(\hat{b}^\dagger + \hat{b})$, where $\hat{b}^\dagger$ ($\hat{b}$) are creation (annihilation) phonon operators, and $z_m = (\hbar/2M\omega_t)^{1/2}$ is the ground state size, with ω_t the trap frequency. The resonance frequency of the optical cavity ω_c^0 is modified by the presence of the dielectric object inside the cavity. A crucial relation is the frequency dependence on the position of the dielectric object, which can be estimated using perturbation theory (see appendix A). This position dependence gives rise to the typical quantum optomechanical coupling,

$$\hat{H}_{\rm OM} = \hbar g(\hat{b}^\dagger + \hat{b})(\hat{a}^\dagger + \hat{a}). \tag{1}$$

Here, $\hat{a}^\dagger$ ($\hat{a}$) are the operators that create (annihilate) a resonant photon in the cavity. The quantum optomechanical coupling g can be written as $g = \sqrt{n_{\rm ph}}g_0$, where $n_{\rm ph}$ is the

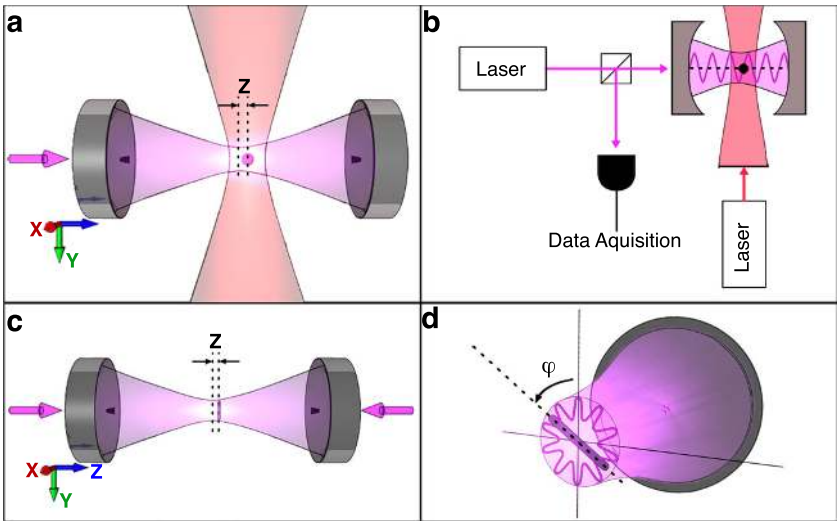

Figure 1. Quantum optomechanics with dielectric objects trapped inside a high-finesse optical cavity. (a) A dielectric sphere is trapped by optical tweezers inside a high-finesse optical cavity. The confinement of the center-of-mass motion along the z-axis is harmonic with frequency ω_t. The driving field generates a radiation pressure able to cool down the mechanical motion to the ground state. (b) Experimental set-up for the trapping and cooling of dielectric spheres using two lasers, one for the driving and one for the trapping. (c) The center-of-mass motion of a dielectric rod can also be trapped and cooled. In this case we assume self-trapping achieved by using two laser modes, see appendix D. (d) The rotational motion of a dielectric rod can also be cooled by generating a standing wave in the azimuthal angle. This can be achieved by superimposing two counterrotating Laguerre–Gauss (LG) modes.

number of photons inside the cavity and $g_0 = z_m \xi_0$ (ξ_0 comes from the resonance frequency dependence on the position, see appendix E). The enhancement of g_0 by a factor of $\sqrt{n_{\rm ph}}$ has been used experimentally to achieve the strong coupling regime in recent experiments with cantilevers [10, 19, 20]. Finally, the total Hamiltonian also includes the mechanical and radiation energy terms as well as the driving of the cavity. See appendix B for details of these terms as well as the derivation of equation (1).

Besides the coherent dynamics given by the total Hamiltonian, there exists also a dissipative part provided by the losses of photons inside the cavity, parametrized by the decaying rate κ, and the heating to the motion of the dielectric object. Remarkably, our objects are trapped without linking the object to other mechanical pieces, and hence thermal transfer does not contribute to the mechanical damping γ. This fact constitutes a distinctive feature of our proposal, possibly yielding extremely high mechanical quality factors. We have investigated in detail the most important sources of decoherence (see appendix F). Firstly, heating due to coupling with other modes, which have very high frequencies, is negligible when having a quadratic potential. Secondly, the maximum pressure required for ground state cooling is $\sim 10^{-6}$ torr, which actually corresponds to the typical one used in optomechanical experiments [13]. The mechanical quality factor of our objects under this pressure is $\sim 10^9$,

and it can be even increased in a higher vacuum. Thirdly, blackbody radiation does not yield a loss of coherence due to 'which-path' information at room temperature and even much higher temperatures [1, 21]. Fourthly, light scattering decreases the finesse of the cavity and produces heat. This sets an upper bound for the size of the objects in the current set-up to be smaller than the optical wavelength. Fifthly, the bulk temperature of the object remains close to the room temperature for sufficiently transparent objects at the optical wavelength, a fact that prevents its damage.

The rotational cooling of cylindrical objects, such as rods (see figure 1(c)), can also be considered. In this case, two counter-rotating LG modes can be employed to create a standing wave in the azimuthal angle ϕ, as illustrated in figure 1(d). The optomechanical coupling is then given by $g_0 = (\hbar/2I\omega_t)\xi_0$, where I is the moment of inertia. Using two modes, one can self-trap both the rotational and the center-of-mass translational motion, and cool either degree of freedom by slightly varying the configuration of the two modes (see appendix E for further details). Both degrees of motion can be simultaneously cooled if the trapping is provided externally (see [22] for a proposal to cool the rotational motion of a mirror and [23] for a recent optomechanical experiment that uses a non-levitating nanorod).

Regarding the feasibility of our scheme, we require the good cavity regime $\omega_t > \kappa$ in order to accomplish ground state cooling [9]–[11]. Moreover, the strong coupling regime $g \gtrsim \kappa, \gamma$ is also required for quantum states generation. Both regimes can be attained with realistic experimental parameters using dielectric spheres and rods. In particular, if one considers fused silica spheres of radius 250 nm in a cavity with finesse 10^5 and length 4 mm, one can obtain $g \sim \kappa \approx 2\pi \times 180$ kHz, and $\omega_t \approx 2\pi \times 350$ kHz. See appendix H for further details.

We tackle now the intriguing possibility to observe quantum phenomena with macroscopic objects. Notably, the optomechanical coupling equation (1) is of the same nature as the typical light–matter interface Hamiltonian in atomic ensembles [2]. Hence, the same techniques can be applied to generate entanglement between Gaussian states of different dielectric objects.

A more challenging step is the preparation of non-Gaussian states, such as the paradigmatic quantum superposition state

$$|\Psi\rangle = \frac{1}{\sqrt{2}}\left(|0\rangle + |1\rangle\right). \tag{2}$$

Here $|0\rangle$ ($|1\rangle$) is the ground state (first excited state) of the quantum harmonic oscillator. In the following, we sketch a protocol to create the state equation (2) —see appendix C for further details. The pivotal idea is to impinge the cavity with a single-photon state, as a result of parametric down conversion followed by a detection of a single photon [24]. When impinging into the cavity, part of the field will be reflected and part transmitted [25]. In the presence of the red-detuned laser, the coupling equation (1) swaps the state of light inside the cavity to the mechanical motional state, yielding the entangled state $|E\rangle_{ab} \sim |\tilde{0}\rangle_a|1\rangle_b + |\tilde{1}\rangle_a|0\rangle_b$. Here a (b) stands for the reflected cavity field (mechanical motion) system, and $|\tilde{0}(\tilde{1})\rangle_a$ is a displaced vacuum (one photon) light state in the output mode of the cavity. The protocol ends by performing a balanced homodyne measurement and by switching off the driving field. The motional state collapses into the superposition state $|\Psi\rangle = c_0|0\rangle + c_1|1\rangle$, where the coefficients $c_{0(1)}$ depend on the measurement result. See figure 2 for the experimental set-up and the results derived in appendix C. This state can be detected by either transferring it back to a new driving field and then performing tomography on the output field, or by monitoring the quantum mechanical oscillation caused by the harmonic trap. Moreover, the amplitude of the oscillation

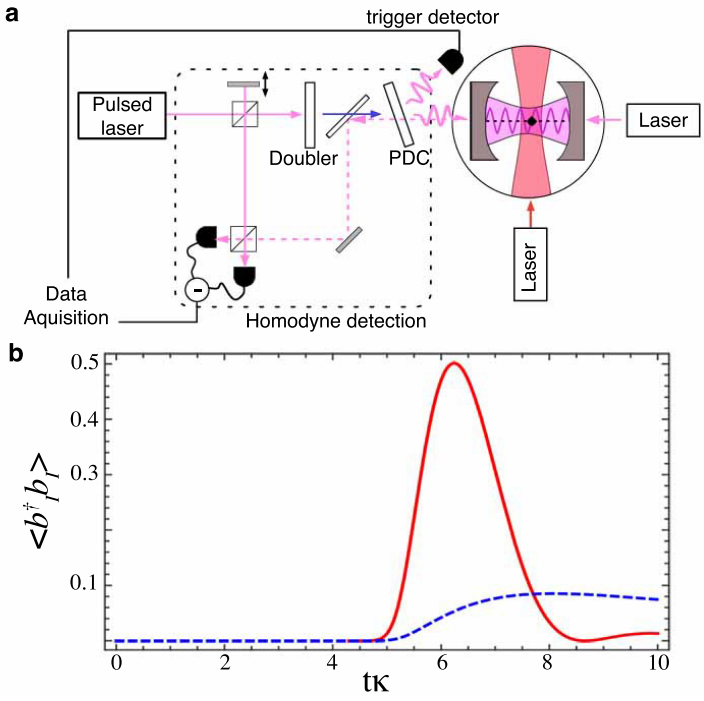

Figure 2. Protocol to prepare quantum superposition states. (a) Experimental set-up for implementing the protocol to prepare the quantum superposition state equation (2). In the figure PDC stands for parametric down conversion and DM for dichroic mirror. A blue photon is converted into two red photons in the PDC. One is detected and the other impinges onto the cavity. If it is reflected, the one photon pulse on top of the driving field goes back through the PDC (which is transparent) and is then reflected downwards toward the homodyne detector by the DM. (b) Mean number of phonons $\langle \hat{b}_{\rm I}^{\dagger}\hat{b}_{\rm I}\rangle$ imprinted to the mechanical oscillator by sending a one-photon pulse to the cavity, see appendix C for details. A Gaussian pulse of width $\sigma = 5.6\,\kappa$ is used. The red solid line corresponds to the strong coupling regime $g = \kappa$, whereas the blue dashed one corresponds to the weak coupling $g/\kappa = 1/4$. In the strong coupling regime, the balanced homodyne measurement should be performed around the time where the mean number of phonons is maximum. This results in the preparation of the quantum superposition state equation (2).

can be amplified by driving a blue-detuned field tuned to the upper motional sideband (see appendix C).

A possible extension of the protocol is to impinge the cavity with other non-Gaussian states, such as the NOON state or the Schrödinger's cat state $|\alpha\rangle + |-\alpha\rangle$ [26], where $|\alpha\rangle$ is a coherent state with phase α, in order to create other quantum superposition states. Furthermore, one can change the laser intensity dynamically to obtain a perfect transmission and avoid the balanced-homodyne measurement; any quantum state of light could be directly mapped to the mechanical system by the time-dependent interaction. Alternatively, one can tune the laser intensity to the upper motional sideband, so that a two-mode squeezing interaction is obtained in the cavity.

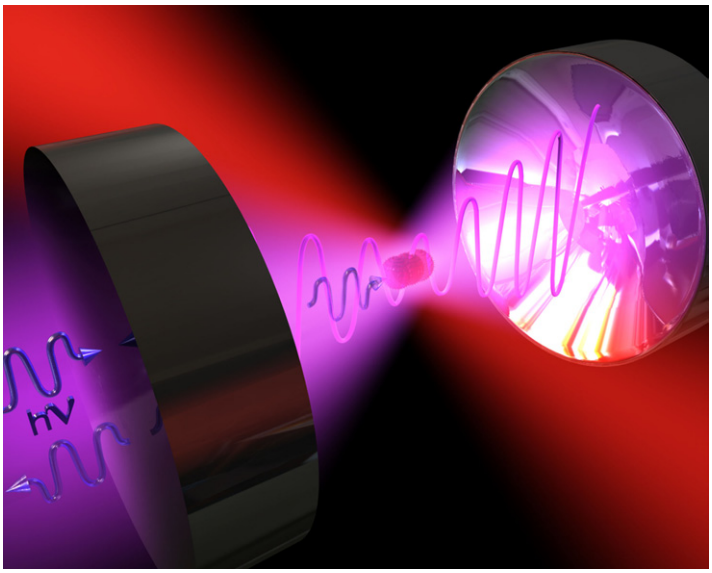

Figure 3. Quantum superposition of living organisms. Illustration of the protocol to create quantum superposition states applied to living organisms, such as viruses, trapped in a high-finesse optical cavity by optical tweezers.

In the bad-cavity limit (relaxing the strong coupling condition) one can use the entanglement between the output mode and the mechanical system to teleport non-Gaussian states (Oriol Romero-Isart *et al*, manuscript in preparation).

In the following, we analyze the possibility of performing the proposed experiment with living organisms. The viability of this perspective is supported by the following: (i) living microorganisms behave as dielectric objects, as shown in optical manipulation experiments in liquids [8]; (ii) some microogranisms exhibit very high resistance to extreme conditions and, in particular, to the vacuum required in quantum optomechanical experiments [7]; (iii) the size of some of the smallest living organisms, such as spores and viruses, is comparable to the laser wavelength, as required in the theoretical framework presented in this work; and (iv) some of them present a transparency window (which prevents the damage caused by the laser's heating) and still have a sufficiently high refractive index. As an example, common influenza viruses, with a size of ~ 100 nm, can be stored for several weeks in vacuum down to 10^{-4} torr [27]. In higher vacuum, up to 10^{-6} torr, a good viability can be foreseen for optomechanics experiments. Due to their structure (e.g. lipid bilayer, nucleocapsid protein and DNA), viruses present a transparency window at the optical wavelength which yields relatively low bulk temperatures [28]. Note that self-trapping or alternative trapping methods, such as magnetic traps, could be used in order to employ lower laser powers. The tobacco mosaic virus (TMV) also presents very good resistance to high vacuum [7], and has a rod-like appearance of 50 nm width and almost 1 μm length. Therefore, it constitutes the perfect living candidate for rotational cooling, see figure 1(d).

In conclusion, we have presented results that open up the possibility of observing genuine quantum effects, such as the creation of quantum superposition states, with nano-dielectric objects and, in particular, with living organisms such as viruses, see figure 3. This entails the possibility of testing quantum mechanics, not only with macroscopic objects but also with living

organisms. A direction to be explored is extension to objects larger than the wavelength (Oriol Romero-Isart *et al* in preparation). This would permit us to bring larger and more complex living organisms to the quantum realm, for instance, the Tardigrade, which have a size ranging from 100 μm to 1.5 mm [29] and is known to survive for several days in open space [30]. We expect the proposed experiments to be a first step in addressing fundamental questions experimentally, such as the role of life and consciousness in quantum mechanics, and perhaps even implications for our interpretations of quantum mechanics [31].

Acknowledgments

We thank M D Lukin for discussions. We acknowledge funding from the Alexander von Humboldt Foundation (to OR-I), the European project SCALA, the DFG FOR635 and the excellence cluster Munich Advanced Photonics–, the Spanish Ministry of Sciences through grants TEC2007-60186/MIC and CSD2007-046-NanoLight.es, Fundació CELLEX Barcelona and Caixa Manresa.

Note added in proof: We have become aware of a recent, similar proposal to optically levitate and manipulate a nanomechanical system by D E Chang *et al* in arXiv:0909.1548.

Appendix A. Resonance frequency dependence on mechanical position

Here we show how to estimate the frequency dependence on the mechanical coordinates of arbitrarily shaped dielectric objects. Note that the resonance frequency ω_c^0, and the optical mode $\varphi_0(\vec{r})$ of the cavity without the dielectric object, are known solutions of the Helmholtz equation. The presence of the dielectric object, which is small compared to the cavity length, can be considered as a tiny perturbation on the whole dielectric present inside the cavity and, thus, a perturbation theory can be used to estimate the resonance frequency

$$\omega_{\rm c}(q) \approx \omega_{\rm c}^0 \left(1 - \frac{\int_{V(q)} (\epsilon_{\rm r} - 1)\, |\varphi_0(\vec{r})|^2 \, {\rm d}\vec{r}}{2 \int |\varphi_0(\vec{r})|^2 \, {\rm d}\vec{r}} \right). \tag{A.1}$$

Here $\epsilon_{\rm r}$ is the relative dielectric constant of the object and $V(q)$ is its volume at coordinates q. The integral in the numerator, which is performed through the volume of the object placed at coordinates q, yields the frequency dependence on q.

Appendix B. Total Hamiltonian in quantum optomechanics

The total Hamiltonian in quantum optomechanics can be typically written as

$$\hat{H}_{\rm t} = \hat{H}_{\rm m} + \hat{H}_{\rm OC} + \hat{H}_{\rm drive}. \tag{B.1}$$

The term $H_{\rm m}$ corresponds to the mechanical energy of the degree of motion $\hat{q} = q_{\rm m}(\hat{b}^\dagger + \hat{b})$, which is assumed to be harmonically trapped. Therefore, $\hat{H}_{\rm m} = \hbar\omega_{\rm t}\hat{b}^\dagger\hat{b}$, where $\omega_{\rm t}$ is the trapping frequency. The driving of the cavity field, with a laser at frequency $\omega_{\rm L}$ and strength E, related to the laser power P by $|E| = \sqrt{2P\kappa/\hbar\omega_{\rm L}}$, is given by

$$\hat{H}_{\rm drive} = {\rm i}\hbar \left(E {\rm e}^{-{\rm i}\omega_{\rm L} t} \hat{a}^\dagger - E^\star {\rm e}^{{\rm i}\omega_{\rm L} t} \hat{a} \right). \tag{B.2}$$

We assumed driving powers for mode-1 of 4 mW. In both cases, one gets the good cavity and strong coupling regimes.

Optical grade fused silica presents very low absorption at 1064 nm, with $\epsilon_1 = 2.1$ and $\epsilon_2 = 2.5 \times 10^{-10}$. In these experimental conditions, the bulk temperature achieved for the dielectric spheres is estimated to be just around four degrees above the room temperature when using the optical tweezers.

References

[1] Arndt M *et al* 1999 Wave-particle duality of c60 molecules *Nature* **401** 680–2

[2] Hammerer K, Sorensen A S and Polzik E S 2008 Quantum interface between light and atomic ensembles arXiv:0807.3358

[3] Marshall W, Simon C, Penrose R and Bouwmeester D 2003 Towards quantum superposition of a mirror *Phys. Rev. Lett.* **91** 130401

[4] Kippenberg T and Vahala K 2008 Cavity optomechanics: back-action at the mesoscale *Science* **321** 1172–6

[5] Marquardt F and Girvin S 2009 Optomechanics *Physics* **2** 40

[6] Favero I and Karrai K 2009 Optomechanics of deformable optical cavities *Nature Photonics* **3** 201–5

[7] Rothschild L J and Mancinelli R L 2001 Life in extreme environments *Nature* **406** 1092–101

[8] Ashkin A and Dziedzic J M 1987 Optical trapping and manipulation of viruses and bacteria *Science* **235** 1517–20

[9] Wilson-Rae I, Nooshi N, Zwerger W and Kippenberg T J 2007 Theory of ground state cooling of a mechanical oscillator using dynamical backaction *Phys. Rev. Lett.* **99** 093901

[10] Marquardt F, Chen J P, Clerk A A and Girvin S M 2007 Quantum theory of cavity-assisted sideband cooling of mechanical motion *Phys. Rev. Lett.* **99** 093902

[11] Genes C, Vitali D, Tombesi P, Gigan S and Aspelmeyer M 2008 Ground-state cooling of a micromechanical oscillator: comparing cold damping and cavity-assisted cooling schemes. *Phys. Rev.* A **77** 033804

[12] Groeblacher S *et al* 2009 Demonstration of an ultracold micro-optomechanical oscillator in a cryogenic cavity *Nat. Phys.* **5** 485–8

[13] Thompson J D *et al* 2008 Strong dispersive coupling of a high-finesse cavity to a micromechanical membrane *Nature* **452** 72–5

[14] Schliesser A, Rivière R, Anetsberger G, Arcizet O and Kippenberg T J 2008 Resolved-sideband cooling of a micromechanical oscillator *Nat. Phys.* **4** 415–19

[15] Mancini S, Man'ko V I and Tombesi P 1997 Ponderomotive control of quantum macroscopic coherence *Phys. Rev.* A **55** 3042–50

[16] Bose S, Jacobs K and Knight P L 1997 Preparation of nonclassical states in cavities with a moving mirror *Phys. Rev.* A **56** 4175–86

[17] Armour A D, Blencowe M P and Schwab K C 2002 Entanglement and decoherence of a micromechanical resonator via coupling to a Cooper-pair box *Phys. Rev. Lett.* **88** 148301

[18] Ashkin A, Dziedzic J M, Bjorkholm J E and Chu S 1986 Observation of a single-beam gradient force optical trap for dielectric particles *Opt. Lett.* **11** 288–90

[19] Groeblacher S, Hammerer K, Vanner M R and Aspelmeyer M 2009 Observation of strong coupling between a micromechanical resonator and an optical cavity field *Nature* **460** 724–7

[20] Dobrindt J M, Wilson-Rae I and Kippenberg T J 2008 Parametric normal-mode splitting in cavity optomechanics *Phys. Rev. Lett.* **101** 263602

[21] Hackermüller L *et al* 2004 Decoherence of matter waves by thermal emission of radiation *Nature* **427** 711–4

[22] Bhattacharya M and Meystre P 2007 Using a Laguerre-Gaussian beam to trap and cool the rotational motion of a mirror *Phys. Rev. Lett.* **99** 153603

[23] Favero I *et al* 2009 Fluctuating nanomechanical system in a high finesse optical microcavity *Opt. Express* **17** 12813–20

[24] Lvovsky A I *et al* 2001 Quantum state reconstruction of the single-photon Fock state *Phys. Rev. Lett.* **87** 050402
[25] Duan L M and Kimble J H 2004 calable Photonic quantum computation through cavity-assisted interactions *Phys. Rev. Lett.* **92** 127902
[26] Ourjoumtsev A, Jeong H, Tualle-Brouri R and Grangier P 2007 Generation of optical 'Schrödinger cats' from photon number states *Nature* **448** 784–6
[27] Greiff D and Rightsel W A 1969 Stabilities of dried suspensions of influenza virus sealed in a vacuum of under different gases *Appl. Microbiol.* **17** 830–5
[28] Steckl A J 2007 DNA—a new material for photonics? *Nat. Photonics* **1** 3–5
[29] Nelson D R 2002 Current status of the tardigrada: evolution and ecology *Int. Comput Biol.* **42** 652–9
[30] Jönsson K I, Rabbow E, Schill R O, Harms-Ringdahl M and Rettberg P 2008 Tardigrades survive exposure to space in low earth orbit *Curr. Biol.* **17** R529–31
[31] Simon C 2009 Conscious observers clarify many worlds arXiv:0908.0322
[32] Hammerer K *et al* 2009 Strong coupling of a mechanical oscillator and a single atom *Phys. Rev. Lett.* **103** 063005
[33] Joos E and Zeh H D 1985 The emergence of classical properties through interaction with the environment *Z. Phys. B: Condens. Matter* **59** 223–43

nature COMMUNICATIONS

OPEN

ARTICLE

Received 5 Jan 2011 | Accepted 2 Mar 2011 | Published 5 Apr 2011

DOI: 10.1038/ncomms1263

Quantum interference of large organic molecules

Stefan Gerlich[1], Sandra Eibenberger[1], Mathias Tomandl[1], Stefan Nimmrichter[1], Klaus Hornberger[2], Paul J. Fagan[3], Jens Tüxen[4], Marcel Mayor[4,5] & Markus Arndt[1]

The wave nature of matter is a key ingredient of quantum physics and yet it defies our classical intuition. First proposed by Louis de Broglie a century ago, it has since been confirmed with a variety of particles from electrons up to molecules. Here we demonstrate new high-contrast quantum experiments with large and massive tailor-made organic molecules in a near-field interferometer. Our experiments prove the quantum wave nature and delocalization of compounds composed of up to 430 atoms, with a maximal size of up to 60 Å, masses up to $m = 6{,}910$ AMU and de Broglie wavelengths down to $\lambda_{dB} = h/mv \simeq 1$ pm. We show that even complex systems, with more than 1,000 internal degrees of freedom, can be prepared in quantum states that are sufficiently well isolated from their environment to avoid decoherence and to show almost perfect coherence.

[1] University of Vienna, Vienna Center for Quantum Science and Technology, VCQ, Faculty of Physics, Boltzmanngasse 5, Vienna 1090, Austria. [2] Max Planck Institute for the Physics of Complex Systems, Nöthnitzer Street 38, Dresden D-01187, Germany. [3] Central Research and Development Department, E. I. DuPont de Nemours & Co. Inc., Experimental Station, PO Box 80328, Wilmington, Delaware 19880-0328, USA. [4] Department of Chemistry, University of Basel, St Johannsring 19, Basel CH-4056, Switzerland. [5] Karlsruhe Institute of Technology, Institute for Nanotechnology, PO Box 3640, Karlsruhe D-76021, Germany. Correspondence and requests for materials should be addressed to M.A. (email: markus.arndt@univie.ac.at).

In many discussions on the foundations of physics, single-particle diffraction at a double slit[1–4] or grating[5–12] is regarded as a paradigmatic example for a highly non-classical feature of quantum mechanics, which has never been observed for objects of our macroscopic world. The quantum superposition principle has become of paramount importance also for the growing field of quantum information science[13]. Correspondingly, research in many laboratories around the world is focusing on our understanding of the role of decoherence for increasingly complex quantum systems and possible practical or truly fundamental limits to the observation of quantum dynamics[14,15].

Here we report on a new leap in quantum interference with large organic molecules. In contrast to earlier successful experiments with internal molecular wave packets,[16] our study focuses on the wave evolution in the centre of mass motion of the molecule as a whole, that is, pure de Broglie interference. We do this with compounds that have been customized to provide useful molecular beams at moderate temperatures[17,18]. Figure 1 compares the size of two perfluoroalkylated nanospheres, PFNS8 and PFNS10, with a single C_{60} fullerene[19] and it relates a single tetraphenylporphyrin molecule (TPP) to its complex derivatives TPPF84 and TPPF152. We demonstrate the wave nature of all these molecules in a three-grating near-field interferometer[20,21] of the Kapitza-Dirac-Talbot-Lau type[22,23], as shown in Figure 2.

Results

Experimental setup. The particles are evaporated in a thermal source. Their velocity is selected using the gravitational free-fall through a sequence of three slits. The interferometer itself consists of three gratings G_1, G_2 and G_3 in a vacuum chamber at a pressure of $p < 10^{-8}$ mbar. The first grating is a SiN_x membrane with 90-nm wide slits arranged with a periodicity of $d = 266$ nm. Each slit of G_1 imposes a constraint onto the transverse molecular position that, following Heisenberg's uncertainty relation, leads to a momentum uncertainty. The latter turns into a growing delocalization and transverse coherence of the matter wave with increasing distance from G_1. The second grating, G_2, is a standing laser light wave with a wavelength of $\lambda = 532$ nm. The interaction between the electric laser light field and the molecular optical polarizability creates a sinusoidal potential, which phase-modulates the incident matter waves. The distance between the first two gratings is chosen such that quantum interference leads to the formation of a periodic molecular density pattern 105 mm behind G_2. This molecular nanostructure is sampled by scanning a second SiN_x grating (G_3, identical to G_1) across the molecular beam while counting the number of the transmitted particles in a quadrupole mass spectrometer (QMS).

In extension to earlier experiments, we have added various technological refinements: the oven was adapted to liquid samples, a liquid-nitrogen-cooled chamber became essential to maintain the source pressure low, a new mass analyser allowed us to increase the detected molecular flux by a factor of four and many optimization cycles in the interferometer alignment were needed to meet all requirements for high-contrast experiments with very massive particles.

Observed interferograms. We recorded quantum interferograms for all molecules of Figure 1, as shown in Figure 3. In all cases the measured fringe visibility V, that is, the amplitude of the sinusoidal modulation normalized to the mean of the signal, exceeds the maximally expected classical moiré fringe contrast by a significant multiple of the experimental uncertainty. This is best shown for TPPF84 and PFNS8, which reached the highest observed interference contrast in our high-mass experiments so far, with individual scans up to $V_{obs} = 33\%$ for TPPF84 ($m = 2{,}814$ AMU) and $V_{obs} = 49\%$ for PFNS8 at a mass of $m = 5{,}672$ AMU. In addition, we have observed a maximum contrast of $V_{obs} = 17 \pm 4\%$ for PFNS10 and $V_{obs} = 16 \pm 2\%$ for TPPF152 (see Figure 3), in which our classical model predicts $V_{class} = 1\%$. This supports our claim of true quantum interference for all these complex molecules.

The most massive molecules are also the slowest and therefore the most sensitive ones to external perturbations. In our particle

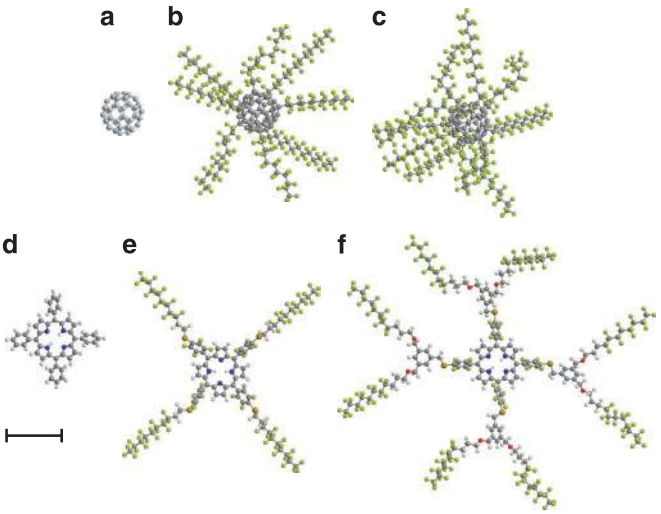

Figure 1 | Gallery of molecules used in our interference study. (**a**) The fullerene C_{60} ($m = 720$ AMU, 60 atoms) serves as a size reference and for calibration purposes; (**b**) The perfluoroalkylated nanosphere PFNS8 ($C_{60}[C_{12}F_{25}]_8$, $m = 5{,}672$ AMU, 356 atoms) is a carbon cage with eight perfluoroalkyl chains. (**c**) PFNS10 ($C_{60}[C_{12}F_{25}]_{10}$, $m = 6{,}910$ AMU, 430 atoms) has ten side chains and is the most massive particle in the set. (**d**) A single tetraphenylporphyrin TPP ($C_{44}H_{30}N_4$, $m = 614$ AMU, 78 atoms) is the basis for the two derivatives (**e**) TPPF84 ($C_{84}H_{26}F_{84}N_4S_4$, $m = 2{,}814$ AMU, 202 atoms) and (**f**) TPPF152 ($C_{168}H_{94}F_{152}O_8N_4S_4$, $m = 5{,}310$ AMU, 430 atoms). In its unfolded configuration, the latter is the largest molecule in the set. Measured by the number of atoms, TPPF152 and PFNS10 are equally complex. All molecules are displayed to scale. The scale bar corresponds to 10 Å.

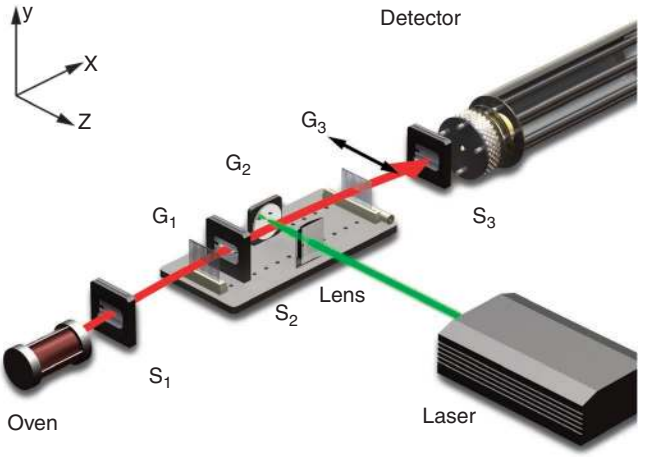

Figure 2 | Layout of the Kapitza-Dirac-Talbot-Lau (KDTL) interference experiment. The effusive source emits molecules that are velocity-selected by the three delimiters S_1, S_2 and S_3. The KDTL interferometer is composed of two SiN_x gratings G_1 and G_3, as well as the standing light wave G_2. The optical dipole force grating imprints a phase modulation $\varphi(x) \propto \alpha_{opt} \cdot P/(v \cdot w_y)$ onto the matter wave. Here α_{opt} is the optical polarizability, P the laser power, v the molecular velocity and w_y the laser beam waist perpendicular to the molecular beam. The molecules are detected using electron impact ionization and quadrupole mass spectrometry.

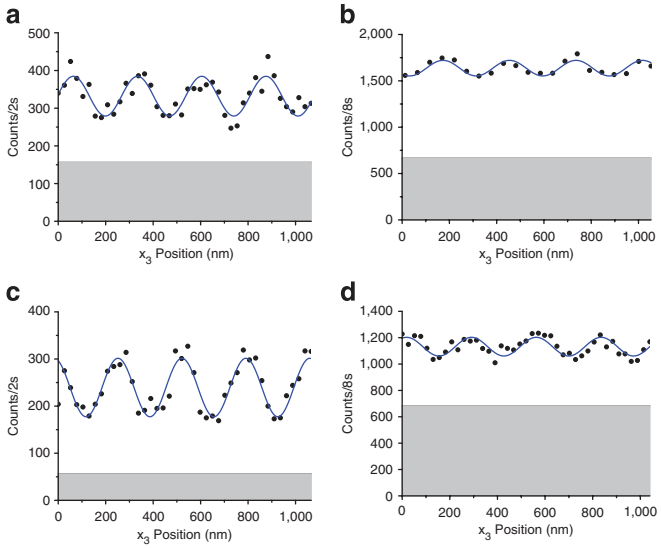

Figure 3 | Quantum interferograms of tailor-made large organic molecules. Quantum interference well beyond the classical expectations has been observed for all molecules in the set. In all panels, the black circles represent the experimental result, the blue line is a sinusoidal fit to the data and the shaded area indicates the detector dark rate. (**a**) The beam of perfluoroalkylated nanospheres, PFNS8, is characterized by a mean velocity of $v = 63\,\mathrm{m\,s^{-1}}$ with a full width $\Delta v_{\mathrm{FWHM}} = 13\,\mathrm{m\,s^{-1}}$. The observed contrast of $V_{\mathrm{obs}} = 49 \pm 6\%$ is in good agreement with the expected quantum contrast of $V_{\mathrm{quant}} = 51\%$ and is clearly discernible from the classically expected visibility of $V_{\mathrm{class}} < 1\%$. The stated uncertainty is the standard deviation of the fit to the data. (**b**) For PFNS10, the signal was too weak to allow a precise velocity measurement and quantum calculation. The oven position for these particles, however, limits the molecular velocity to $v < 80\,\mathrm{m\,s^{-1}}$ and therefore allows us to define an upper bound to the classical visibility. (**c**) For TPPF84, we measure $v = 95\,\mathrm{m\,s^{-1}}$ with $\Delta v_{\mathrm{FWHM}} = 34\,\mathrm{m\,s^{-1}}$. This results in $V_{\mathrm{obs}} = 33 \pm 3\%$ with $V_{\mathrm{quant}} = 30\%$ and $V_{\mathrm{class}} < 1\%$. (**d**) The signal for TPPF152 is equally low compared with that of PFNS10. For this compound we find $V_{\mathrm{obs}} = 16 \pm 2\%$, $V_{\mathrm{quant}} = 45\%$ and $V_{\mathrm{class}} = 1\%$.

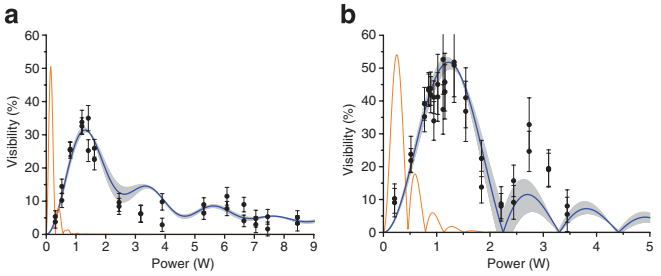

Figure 4 | Quantum interference visibility as a function of the diffracting laser power. The best distinction between quantum and classical behaviour is made by tracing the interference fringe visibility as a function of the laser power, which determines the phase imprinted by the second grating. Each of the two experimental runs per molecule is represented by full circles and the error bar provides the 68% confidence bound of the sinusoidal fit to the interference fringe. The thick solid line is the quantum fit in which the shaded region covers a variation of the mean molecular velocity by $\Delta v = \pm 2\,\mathrm{m\,s^{-1}}$. (**a**) The TPPF84 data are well reproduced by the quantum model (see text) and completely missed by the classical curve (thin line on the left). (**b**) The same holds for PFNS8. The following parameters were used for the models: TPPF84: $v = 95\,\mathrm{m\,s^{-1}} \pm 16\%$, $\alpha = 200\,\mathrm{Å^3} \times 4\pi\varepsilon_0$ (fit), $\sigma_{\mathrm{opt}} = 10^{-21}\,\mathrm{m^{-2}}$, $w_x = 34 \pm 3\,\mu\mathrm{m}$ and $w_y = 500 \pm 50\,\mu\mathrm{m}$. PFNS8: $v = 75\,\mathrm{m\,s^{-1}} \pm 10\%$, $\alpha = 190\,\mathrm{Å^3} \times 4\pi\varepsilon_0$ (fit), $\sigma_{\mathrm{opt}} = 10^{-21}\,\mathrm{m^{-2}}$, $w_x = 27 \pm 3\,\mu\mathrm{m}$ and $w_y = 620 \pm 50\,\mu\mathrm{m}$.

set, these are PFNS10 and TPPF152, which, in addition, exhibited the smallest count rates and therefore the highest statistical fluctuations. To record the interferograms, we had to open the vertical beam delimiter S_2 and accept various imperfections: an increased velocity spread, a higher sensitivity to grating misalignments and also an averaging over intensity variations in the Gaussian-shaped diffraction laser beam G_2. In addition, we had to enhance the QMS transmission efficiency at the expense of transmitting a broader mass range. The recorded signals associated with PFNS10 and TPPF152 covered a mass window of $\Delta m_{\mathrm{FWHM}} = 500\,\mathrm{AMU}$ around their nominal masses. Although all samples were well characterized before the evaporation process, we can therefore not exclude some contamination with adducts or fragments in this high mass range. But even if there were a relative mass spread of 10%, this would only influence the wavelength distribution $\Delta\lambda_{\mathrm{dB}}/\lambda_{\mathrm{dB}}$ the same way as does the velocity spread. Owing to the inherent design of the Kapitza-Dirac-Talbot-Lau interferometer[22], these experimental settings are still compatible with sizeable quantum interference, even under such adverse conditions.

Comparison of theory and experiment. The experimental values have to be compared with the theoretical predictions based on a classical and a quantum model[23]. The measured interference visibility is plotted as a function of the diffracting laser power P in Figure 4 for TPPF84 (4a) and PFNS8 (4b). Our data are in very good agreement with the full quantum calculation and in clear discrepancy with the classical prediction. The abscissa scaling of the $V(P)$ curve is a good indicator for that. The quantum prediction mimics the classical curve qualitatively, but it is stretched in the laser power by a factor of about six (see Methods).

The laser power can be calibrated with an accuracy of ±1% but the abscissa also scales in proportion to the optical molecular polarizability and inversely with the vertical laser waist. The theoretical curves of Figure 4 are plotted assuming $\alpha_{\mathrm{opt}} = 200\,\mathrm{Å^3} \times 4\pi\varepsilon_0$ for TPPF84 and $\alpha_{\mathrm{opt}} = 190\,\mathrm{Å^3} \times 4\pi\varepsilon_0$ for PFNS8. These numbers have to be compared with the static polarizabilities computed using Gaussian09 (ref. 24). These are $\alpha_{\mathrm{stat}} = 155\,\mathrm{Å^3} \times 4\pi\varepsilon_0$ for TPPF84 and $\alpha_{\mathrm{stat}} = 200\,\mathrm{Å^3} \times 4\pi\varepsilon_0$ for PFNS8. A variation in the polarizability changes the horizontal scale of the plot as does a different laser waist. Both are bound by a relative uncertainty of less than 30%. A classical explanation is therefore safely excluded as an explanation for the experiments.

The quantitative agreement of the experimental and expected contrast is surprisingly good, given the high complexity of the particles. Various factors contribute to the remaining small discrepancies. The interference visibility is highly sensitive to apparatus vibrations, variations in the grating period on the level of 0.5 Å and a misalignment below 100 µrad in the grating roll angle.

Discussion

PFNS10 and TPPF152 contain 430 atoms covalently bound in one single particle. This is ~350% more than that in all previous experiments[25] and it compares well with the number of atoms in small Bose–Einstein condensates[26] (BEC), which, of course, operate in a vastly different parameter regime: The molecular de Broglie wavelength λ_{dB} is about six orders of magnitude smaller than that of ultracold atoms and the internal molecular temperature exceeds typical BEC values ($T < 1\,\mu\mathrm{K}$) by about nine orders of magnitude. Although matter wave interference of BECs relies on the de Broglie wavelength of the individual atoms, our massive molecules always appear as single entities.

One can find various definitions in the literature for what a true Schrödinger cat[27] should be and a number of intriguing experiments have reported the generation of photonic[28] or atomic cat-states[29,30].

In as far as the term designates the quantum superposition of two macroscopically distinct states of a highly complex object, the molecules in our new experimental series are among the fattest Schrödinger cats realized to date. Schrödinger reasoned whether it is possible to bring a cat into a superposition state of being 'dead' *and* 'alive'. In our experiment, the superposition consists of having all 430 atoms simultaneously 'in the left arm' and 'in the right arm' of our interferometer, that is, two possibilities that are macroscopically distinct. The path separation is about two orders of magnitude larger than the size of the molecules.

Schrödinger's thought experiment originally also required the entanglement between a microscopic atom and the final state of the macroscopic cat. Such a mechanism is not needed to create the molecular superposition state in our experiment. Entanglement between a molecule and a microscopic probe particle does, however, occur in decoherence processes in which the quantum interaction with the environment reveals *which-path* information[14,15] and destroys the interference pattern. Collisions with residual gas molecules[31], the emission of heat radiation[32] and the absorption of blackbody radiation are among the most important decoherence mechanisms for interferometry with massive particles. We estimate that they lead to a visibility reduction of less than 1% under the conditions of the present experimental arrangement, in spite of the high internal molecular temperatures and substantial dipole fluctuations.

Specifically for PFNS8, a microscopically realistic account of the decoherence processes[31,32] predicts a visibility reduction of 10% only if the temperature of either the molecule or the radiation field exceeds 1,500 K, or if the residual nitrogen gas pressure exceeds 2×10^{-7} mbar.

In conclusion, our experiments reveal the quantum wave nature of tailor-made organic molecules in an unprecedented mass and size domain. They open a new window for quantum experiments with nanoparticles in a complexity class comparable to that of small proteins, and they demonstrate that it is feasible to create and maintain high quantum coherence with initially thermal systems consisting of more than 1,000 internal degrees of freedom.

Methods

Chemical synthesis. The porphyrin derivatives were synthesized by the attachment of a highly fluorous thiol to meso-tetra(pentafluorophenyl)porphyrin in a nucleophilic aromatic substitution reaction by applying a modified literature procedure[33]. To assemble TPPF84, the commercially available 1*H*,1*H*,2*H*,2*H*-perfluorododecane-1-thiol as nucleophilic fluorous part was introduced to the porphyrin unit. The branched thiol building block for TPPF152 was synthesized in three reaction steps. A reaction sequence including mono-functionalization of tris(bromomethyl)benzene with a protected thiol, introduction of two fluorous ponytails and a final deprotection of the thiol functionality yielded the desired fluorous thiol suitable for the envisaged substitution reaction. All target structures were purified by column chromatography and characterized by nuclear magnetic resonance spectroscopy and mass spectrometry (Supplementory Methods).

Differences between the classical and quantum predictions. The functional dependence of the interference fringe visibility on the laser power is qualitatively similar in both a classical and a full quantum treatment. As observed from the treatment described in ref. 23 the abscissa scaling differs, however, by the factor $\xi/\sin(\xi)$ with $\xi = \pi \cdot L/L_T$, where L is the distance between two consecutive gratings and $L_T = d^2/\lambda_{dB}$ is the Talbot length. For the case of Figure 4, we find $\xi/\sin(\xi) \simeq 5.9$. The experimental data are in clear agreement with the quantum model.

Equipment. The diffracting laser beam is generated by a Coherent Verdi V18 laser at 532 nm. The QMS is an Extrel CMS with a rod diameter of 9.5 mm, operated at a radio frequency of 440 kHz. The SiN_x gratings in G_1 and G_3 were made by Dr Tim Savas, nm² LLC & MIT Cambridge.

References

1. Zeilinger, A., Gähler, R., Shull, C. G., Treimer, W. & Mampe, W. Single- and double-slit diffraction of neutrons. *Rev. Mod. Phys.* **60,** 1067–1073 (1988).
2. Carnal, O. & Mlynek, J. Young's double-slit experiment with atoms: a simple atom interferometer. *Phys. Rev. Lett.* **66,** 2689–2692 (1991).
3. Zimmermann, B. *et al.* Localization and loss of coherence in molecular double-slit experiments. *Nat. Phys.* **4,** 649–655 (2008).
4. King, B., Di Piazza, A. & Keitel, C. H. A matterless double slit. *Nat. Photonics* **4,** 92–94 (2010).
5. Hasselbach, F. Progress in electron- and ion-interferometry. *Rep. Prog. Phys.* **73,** 016101 (2010).
6. Rauch, H. & Werner, A. *Neutron Interferometry: Lessons in Experimental Quantum Mechanics* (Oxford University, 2000).
7. Adams, C. S., Sigel, M. & Mlynek, J. Atom optics. *Phys. Rep.* **240,** 143–210 (1994).
8. Keith, D. W., Schattenburg, M. L., Smith, H. I. & Pritchard, D. E. Diffraction of atoms by a transmission grating. *Phys. Rev. Lett.* **61,** 1580–1583 (1988).
9. Cronin, A. D., Schmiedmayer, J. & Pritchard, D. E. Optics and interferometry with atoms and molecules. *Rev. Mod. Phys.* **81,** 1051–1129 (2009).
10. Arndt, M. *et al.* Wave-particle duality of C_{60} molecules. *Nature* **401,** 680–682 (1999).
11. Hackermüller, L. *et al.* Wave nature of biomolecules and fluorofullerenes. *Phys. Rev. Lett.* **91,** 090408 (2003).
12. Brühl, R *et al.* Diffraction of neutral helium clusters: evidence for 'magic numbers'. *Phys. Rev. Lett.* **92,** 185301 (2004).
13. Ladd, T. D., Jelezko, F., Laflamme, R., Nakamura, Y., Monroe, C. & O'Brien, J. L. Quantum computers. *Nature* **464,** 45–53 (2010).
14. Zurek, W. H. Decoherence, einselection, and the quantum origins of the classical. *Rev. Mod. Phys.* **75,** 715–775 (2003).
15. Joos, E. *et al. Decoherence and the Appearance of the Classical World in Quantum Theory* (Springer, 1996).
16. Ohmori, K. Wave-packet and coherent control dynamics. *Annu. Rev. Phys. Chem.* **60,** 487–511 (2009).
17. Fagan, P. *et al.* Production of perfluoroalkylated nanospheres from buckminsterfullerene. *Science* **262,** 404–407 (1993).
18. Deachapunya, S. *et al.* Slow beams of massive molecules. *Eur. Phys. J. D.* **46,** 307–313 (2008).
19. Kroto, H. W., Heath, J. R., O'Brian, S. C., Curl, R. F. & Smalley, R. E. C60: Buckminsterfullerene. *Nature* **318,** 162–163 (1985).
20. Clauser, J. F. in *Experimental Metaphysics* (eds Cohen, R.S., Home, M. & Stachel, J.) 1–11 (Kluwer Academic, 1997).
21. Brezger, B., Arndt, M. & Zeilinger, A. Concepts for near-field interferometers with large molecules. *J. Opt. B* **5,** S82–S89 (2003).
22. Gerlich, S. *et al.* A Kapitza-Dirac-Talbot-Lau interferometer for highly polarizable molecules. *Nature Physics* **3,** 711–715 (2007).
23. Hornberger, K. *et al.* Theory and experimental verification of Kapitza-Dirac-Talbot-Lau interferometry. *New J. Phys.* **11,** 043032 (2009).
24. Frisch, M. J. *et al.* Gaussian 09, Revision A.1. (Gaussian, Inc., Wallingford CT, 2009).
25. Tüxen, J., Gerlich, S., Eibenberger, S., Arndt, M. & Mayor, M. Quantum interference distinguishes between constitutional isomers. *Chem. Comm.* **46,** 4145–4147 (2010).
26. Bradley, C. C., Sackett, C. A., Tollett, J. J. & Hulet, R. G. Evidence of Bose-Einstein condensation in an atomic gas with attractive interactions. *Phys. Rev. Lett.* **79,** 1170 (1997).
27. Schrödinger, E. Die gegenwärtige Situation in der Quantenmechanik. *Naturwissenschaften* **23,** 844–849 (1935).
28. Brune, M. *et al.* Observing the progressive decoherence of the 'meter' in a quantum measurement. *Phys. Rev. Lett.* **77,** 4887–4890 (1996).
29. Leibfried, D. *et al.* Creation of a six-atom 'Schrödinger Cat' state. *Nature* **438,** 639–642 (2005).
30. Monz, T. *et al.* Coherence of large-scale entanglement. arXiv:1009.6126v1 [quant-ph] (2010).
31. Hornberger, K. *et al.* Collisional decoherence observed in matter wave interferometry. *Phys. Rev. Lett.* **90,** 160401 (2003).
32. Hackermüller, L. *et al.* Decoherence of matter waves by thermal emission of radiation. *Nature* **427,** 711–714 (2004).
33. Samaroo, D., Vinodu, M., Chen, X. & Drain, C. M. Meso-tetra(pentafluorophenyl)-porphyrin as an efficient platform for combinatorial synthesis and the selection of new photodynamic therapeutics using a cancer cell line. *J. Comb. Chem.* **9,** 998–1011 (2007).

Acknowledgments

We thank Lucia Hackermüller (now University of Nottingham) for important contributions to the setup of a first version of this experiment until the end of 2006, and Hendrik Ulbricht (now University of Southampton) for his collaboration until 2008. We thank Anton Zeilinger for his role as an initiator of the 'foundations of quantum physics' research programme in Vienna. The interference experiments were financed through the Austrian FWF Wittgenstein grant (Z149-N16), the doctoral

program CoQuS (Grant W1210-N16). The chemical synthesis in Basel was funded by the Swiss National Science Foundation and the NCCR 'Nanoscale Science'. The groups in Vienna, Basel and Dresden were supported by the ESF EuroCore Program MIME (I146-N16).

Author contributions

S.G. and S.E. performed all interference experiments as well as the analysis of the data with important contributions by M.T. M.A. contributed at various stages of the experiment. J.T. synthesized, purified and analysed the porphyrin derivatives based on a design developed together with M.M. P.F. provided the perfluoroalkylated nanospheres. M.A. and M.M. initiated and coordinated the experiments. S.N. and K.H. participated in the interpretation of the data. M.A., S.G. and S.N. wrote the paper. All authors discussed the results and commented on the manuscript.

Additional information

Supplementary Information accompanies this paper at http://www.nature.com/naturecommunications

Competing financial interests: The authors declare no competing financial interests.

Reprints and permission information is available online at http://npg.nature.com/reprintsandpermissions/

How to cite this article: Gerlich, S. *et al.* Quantum interference of large organic molecules. *Nat. Commun.* 2:263 doi: 10.1038/ncomms1263 (2011).